Progress In Electromagnetics Research, Vol. 159, 93–124, 2017

Illumination Optics in Emerging Naked-Eye 3D Display

Aiqin Zhang[1], Jiahui Wang[1], Yangui Zhou[1, 2], Haowen Liang[1],
Hang Fan[3], Kunyang Li[1], Peter Krebs[1], and Jianying Zhou[1, 4, *]

(*Invited Review*)

Abstract—Illumination optics in emerging naked-eye 3D display, especially in time-spatial multiplexing, or directional backlight naked-eye 3D display system, is systematically examined. Key issues in directional backlight system include: 1) Directional transmission of the left- and right-eye images to the corresponding viewing zone with small crosstalk; 2) The luminance on the screen should be homogeneous even for the viewers moving around. In this paper, we propose an adaptive optimization solution based on root mean square (RMS) for the design of illumination optics of the naked-eye 3D system. Based on the designed free-form backlight illumination, the overall design schemes for both single-user and multi-user naked-eye 3D display are proposed and demonstrated. By utilizing the novel dynamic synchronized backlight technique, the temporal crosstalk is effectively brought into control. The display defects such as the dark bands appearing at the joints of the lens array or at the middle of the Fresnel lens are simulated numerically and tested experimentally, hence providing effective design guidelines for the optical components as well as their fabrication error tolerance. Additionally, we propose a continuous backlight technique to improve the luminance homogeneity. Furthermore, a quantitative evaluation mechanism for the moiré pattern based on the Fourier analysis method, by introducing the contrast sensitivity function (CSF), is presented. A novel arrangement of a quasi-random RGB sub-pixel array is proposed to reduce the visibility of moiré pattern. As a result, full HD glassless 3D display suitable for glassless virtual and augmented realities is demonstrated with an unprecedented display quality.

1. INTRODUCTION

Naked-eye 3D display has attracted a great deal of interest for over 100 years since it can create 3D vision without requiring the viewers to wear extra equipment such as glasses or helmets [1, 2]. The application of naked-eye 3D display is very broad ranging from consumer electronics to various industrial and medical equipment [3]. Variety of 3D products such as naked-eye 3D mobile phone, panel display, television, and digital photo frame, are now appearing on the market. There have been different kinds of technologies to realize naked-eye 3D display, including holographic display [4–6], volumetric display [7–9], and auto-stereoscopic display [10–15]. Holographic display is regarded as a powerful technique for naked-eye 3D display. Before becoming a widely accepted technique, holographic display needs to overcome the challenges imposed by the responding materials and by mega-data transmission required for recording and displaying. On the other hand, auto-stereoscopic display appears to become a mainstream of naked-eye 3D display, for its compatibility with the existing liquid crystal display (LCD) technology supported by matured production chain. The autostereoscopic technology is further assisted on the internet by a

---

Received 1 June 2017, Accepted 3 July 2017, Scheduled 24 July 2017

* Corresponding author: Jianying Zhou (stszjy@mail.sysu.edu.cn).
[1] State Key Laboratory of Optoelectronic Materials and Technology, Sun Yat-sen University, Guangzhou 510275, China. [2] School of Physics and Optoelectronic Engineering, Foshan University, Foshan 528000, China. [3] Midstereo, Inc. Co., Guangzhou 510275, China.
[4] SYSU-CMU Shunde International Joint Research Institute, Shunde 528300, China.

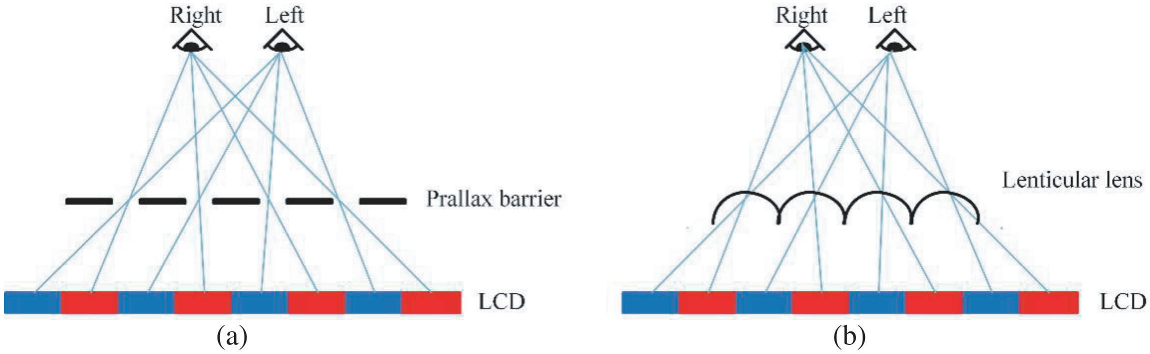

Figure 1. Top view of the spatial-multiplexing method for naked-eye 3D display, (a) based on parallax barrier and (b) based on lenticular lens.

large number of existing 3D resources such as 3D film and 3D TV channels thanks to today's advanced broadband communication technology.

It is well known by physiologic study that stereoscopic vision is mainly produced by binocular parallax, motion parallax, accommodation and convergence of human eyes [16, 17]. The basic principle for auto-stereoscopic 3D display is to project the left and right eye parallax images to the corresponding eyes, which can be realized by the technique of either spatial-multiplexing or time-spatial multiplexing [18]. As shown in Fig. 1, the usual approach is to put a parallax barrier [19–21] or lenticular lens [22] as a spatial-multiplexing component. In these systems, the pixels colored as blue on the LCD will display the left eye image, and the right eye image will be loaded simultaneously by the pixels colored as red. By introducing the parallax barrier or lenticular lens between the LCD and viewer, the left and right eyes of the viewer will respectively receive the corresponding images, and then the stereoscopic vision will be obtained by the fusional convergence process of brain. For the parallax barrier approach, the resolution and brightness of the image seen by each eye will be degraded in half. This degradation will increase as the number of viewing points is increased. Even though the brightness can be improved by a lenticular lens array as a spatial-multiplexing device, the problem of the resolution reduction still exists. By employing an ultrahigh definition LCD such as 4 K or 8 K, the resolution can be increased. Nevertheless, not only a higher cost, but also a more accurate alignment on the pixel level over the entire screen will be required.

In order to overcome the resolution-reduction in the spatial-multiplexing technology, the time-spatial multiplexing method [13] is proposed, as shown in Fig. 2. The LCD only loads left or right eye image at a certain time, which is different from the loading in spatial-multiplexing system. Thus each eye receives the full resolution of the display. The switching frequency of light source should be

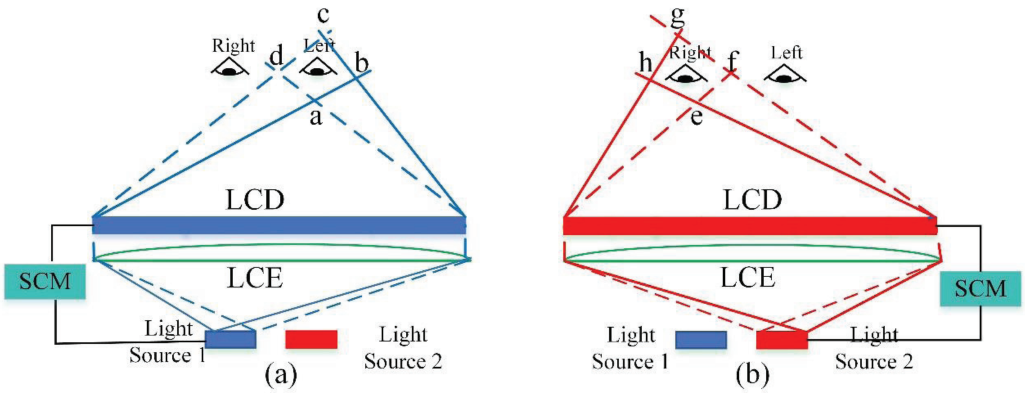

Figure 2. Top view of the optical schematic diagram for time-spatial multiplexing naked-eye 3D display, while turning on (a) light source 1 and (b) light source 2, sequentially.

synchronous with the refreshing rate of LCD. Therefore, a synchronous circuit module (SCM) is needed to simultaneously control the LCD and the light sources. The required frequency should be more than 120 Hz to avoid blinking phenomenon according to the persistence of vision [23].

The basic optical principle for the proposed time-spatial multiplexing naked-eye 3D display can be explained as follows. Light emitting from light source 1 as shown in Fig. 2(a) will firstly pass through the light concentrating equipment (LCE) and then go through the LCD. At the same time, the left eye image will be loaded on LCD. Only within the zone surrounded by a, b, c and d, (here called left viewing zone), the eye of viewer can receive the whole image on LCD, otherwise, the partial one. For example, the light emitting from a point at left edge of the light source 1 will illuminate the whole surface of LCD in front of LCE as shown in Fig. 2(a) and then focus at point b by the convergence of LCE. Similarly, when turning on light source 2 shown in Fig. 2(b), it works in a similar way as expressed for left viewing zone. We can see that the LCE plays a very important role in the time-spatial multiplexing naked-eye 3D display. The light sources are arranged at proper positions behind LCE and focus at different zones after illuminating the LCD. Furthermore, the proposed time-spatial multiplexing naked-eye 3D display can not only offer the full resolution display but also form multi-view zones by inserting more light sources units behind LCE with suitable arrangement. This back-light directional naked-eye 3D display, as it does with other autostereoscopic display, presents some basic technological difficulties, such as the unacceptable crosstalk, visible moiré pattern, non-uniformity of luminance on the screen, among others.

In the application of the proposed single-user naked-eye 3D display based on time-spatial multiplexing technology, the viewer may move around during viewing process, and the movement might be large or small. It will not have obvious influence on the viewer if the viewer's pupils remain within a particular viewing zone. However, the 3D viewing experience will be spoiled or disappeared when the pupils are located at the edges or out of the viewing zone. Hence, it is necessary to make the viewing zones switchable to track the eyes movement. In other words, we need to establish flexible viewing zones which are viewer's pupils dependent. Hence an eye-tracking technology has to be adopted to address this issue. In a multi-user system where there are more than two viewers, a multi-user naked-eye 3D is necessary.

In the following paragraph, we will introduce theoretical basis for designing the proposed time-spatial multiplexing naked-eye 3D display. The LCE converging the light from different light sources to different viewing zones is an essential device in the naked-eye 3D system. The theory for designing the LCE will be analyzed. The arrangement of backlight sources will be described in detail. Additionally, the approaches to solve the issues related to the crosstalk, luminance homogeneity, and with moiré pattern will be presented.

2. OPTICAL DESIGN FOR NAKED-EYE 3D DISPLAY

2.1. Design Theory for Fresnel Lens

In the proposed time-spatial multiplexing naked-eye 3D display system, the light illuminating on LCD should be diverted to the designated viewing zones, which can be realized by importing an LCE between the light source and LCD. Usually, Fresnel lens is used as an LCE, for the advantages of reduced thickness and light weight. The general theory for designing Fresnel lens is derived by the following process.

Figure 3 represents the light path diagram for a Fresnel lens which has a flat surface and an uneven surface composed by several triangular teeth. We assume that a point light source is placed at the point F on the optical axis of Fresnel lens. Light rays emitting from this source will finally focus at point F' on the other side of the Fresnel lens. The light ray n, with an angle of μ_n to the optical axis, will make the first refraction at point A and the second at point B on any teeth as shown in Fig. 3(b), and finally intersects with optical axis at point F'. The relationship maong $\theta_n, \theta_n', \beta_n$ and β_n' will satisfy formula (1) according to the Snell's law.

$$\frac{\sin\theta_n}{\sin\theta_n'} = \frac{\sin\beta_n}{\sin\beta_n'} = \frac{N_2}{N_1} = N \tag{1}$$

where N_1 and N_2 respectively represent the refractive indices of air and Fresnel lens. From the figure, expression (2) can be obtained by a geometrical relationship.

$$\theta_n = \mu_n + \alpha_n; \quad \alpha_n = \theta_n' + \beta_n; \quad \beta_n' = \mu_n' \tag{2}$$

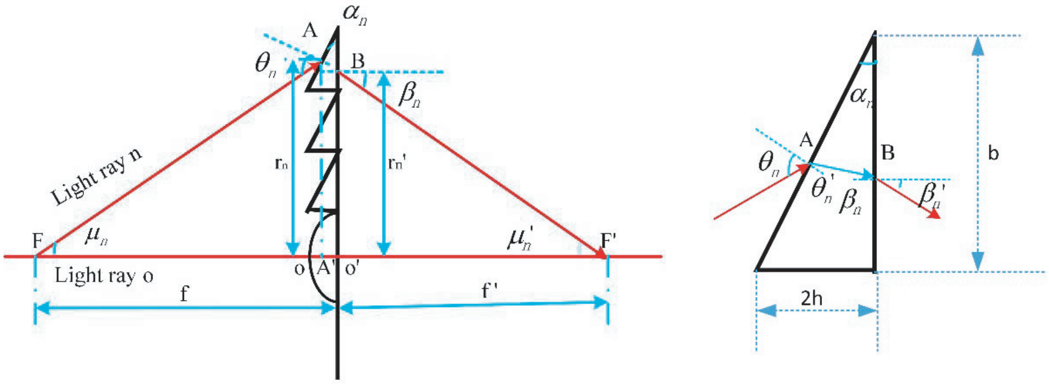

(a) (b)

Figure 3. (a) The optical pathway diagram of Fresnel lens, (b) the zoom in beam path on a particular pitch.

where α_n labeled in Fig. 3(b) is the included angle of the slope facet and flat surface of Fresnel lens. μ_n, $\mu_n^{'}$ are the angle formed by the incident and refracted ray with the optical axis $FF^{'}$. Based on the above formulas, the function of α_n is expressed by

$$\mathrm{tg}\alpha_n = \frac{\sin\mu_n^{'} + \sin\mu_n}{\sqrt{N^2 - \sin^2\mu_n^{'}} - \cos\mu_n} \tag{3}$$

As shown in the picture, FA$^{'}$=FO$^{'}$−A$^{'}$O$^{'}$ $= f-$A$^{'}$O$^{'}$ $= f - h$, and A$^{'}$O$^{'}$ $= h$ which is vertical dimension of middle point A of slope side to bottom side of the triangular piece, whose bottom size is represented as b. Thus,

$$\left.\begin{aligned} \sin\mu_n &= r_n \Big/ \sqrt{(f-h)^2 + r_n^2} \\ \cos\mu_n &= (f-h) \Big/ \sqrt{(f-h)^2 + r_n^2} \\ \sin\mu_n^{'} &= r_n^{'} \Big/ \sqrt{f'^2 + r_n'^2} \end{aligned}\right\} \tag{4}$$

r_n and $r_n^{'}$ respectively represent the distances of points A and B to the optical axis OO$^{'}$; f and $f^{'}$ respectively denote the distances of point F and F' to the point O$^{'}$. Inserting Equations (4) to Eq. (3), angle α_n can be calculated by Eq. (5).

$$\mathrm{tg}\alpha_n = \frac{r_n^{'} \Big/ \sqrt{f'^2 + r_n'^2} + r_n \Big/ \sqrt{(f-h)^2 - r_n^2}}{\sqrt{N^2 - r_n'^2/(f'^2 + r_n'^2)} - (f-h) \Big/ \left[\sqrt{(f-h)^2 + r_n^2}\right]} \tag{5}$$

Equations (3), (4) and (5) can be used as the universal formulas for designing the Fresnel lens. Beginning with the given demands such as the light source distance f, view distance $f^{'}$, width b or depth h of a pitch, the other parameters of the Fresnel lens such as the angle α_n of the pitches can be obtained based on the above universal formulas. Thus the Fresnel lens can be fabricated based on the obtained parameters. When the value of h keeps unchanged for all the triangular pieces, the Fresnel lens can be called as equal-depth Fresnel lens. If the value of b is set as a constant, the Fresnel lens can be called as equal-width Fresnel lens. By rotating or translating the designed cross section of Fresnel lens, we can obtain an annular or a linear Fresnel lens.

2.2. Design Method for Backlight Module

In the naked-eye 3D display, a series of light emitting diodes (LEDs) are used as the light source for the advantages of energy efficiency, long service life, and low heat dissipation. Fig. 4 shows the top

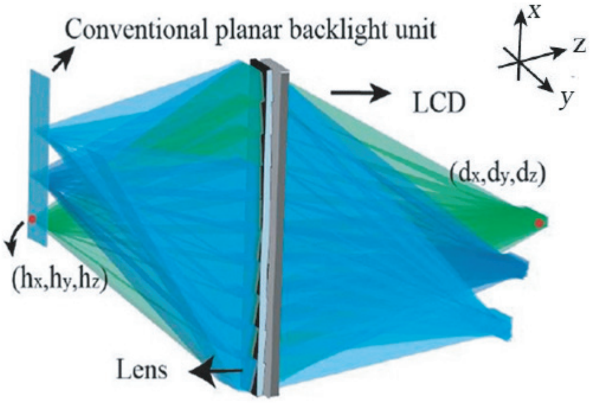

Figure 4. Top view of a traditional planar backlight system, x-y plane is parallel to the LCD, z-axis is perpendicular to the LCD.

view of a conventional planar backlight system, which consists of a planar backlight unit, a Fresnel lens and an LCD panel. The planar backlight unit can be treated as a planar light source composed by a series of point light sources (PLSs). Thus the viewing zone can be regarded as the area consisting of the corresponding image points of those PLSs.

In a practical optical system, extended spots will be generated in the viewing plane instead of an ideal point for the PLS by just considering the refraction and reflection of the Fresnel lens and by ignoring the contributions from diffraction and scattering. For the off-axis PLS, the size of the defocused spots will be increased, and the distance to Fresnel lens will be decreased as demonstrated in Fig. 4. If the size of defocused spots is extended to a level so that it is greater than the pupil size, it causes parts of the rays escaping from the entrance of the pupil, and the perceived luminance homogeneity may decrease.

In order to obtain good viewing experience, all the light emitting from a PLS is required to bring to the ideal image point after passing though the Fresnel and LCD. Only the spot size is confined within the pupil size, and the visual perception could be in acceptable level. Therefore, all PLSs should be arranged in such a way to achieve that objective. Here we propose an adaptive optimization solution to design the backlight unit based on the RMS value of a spot [24].

For a fixed viewing distance of d_z in front of the LCD, the formula of RMS of a spot used to calculated the size of defocused spots can be expressed as

$$\mathrm{RMS}^2\left(\vec{h},\vec{d}\right)=\sum_{j=1}^{n}\frac{1}{n}\left\{\left[X\left(\vec{h},\lambda,j\right)-d_y\right]^2+\left[Y\left(\vec{h},\lambda,j\right)-d_y\right]^2\right\} \tag{6}$$

where n is the number of light rays emitted by a PLS; j denotes any light ray; λ is the wavelength of light ray; (X, Y) is the coordinate value of light ray j on the x-y planes. Essentially, for any given view point (d_x, d_y, d_z), the purpose of backlight design is to determine the coordinate value of point (h_x, h_y, h_z) to place the PLS, so that the RMS^2 reaches a minimum value. After calculating all the corresponding coordinate values of PLSs, for all viewing points within the given viewing zone, the backlight shape can be acquired.

As an example of the proposed method, we set the viewing distance at 900 mm in front of the LCD, and an annular Fresnel lens with a focal length of 180 mm is inserted to be an LCE. The other parameters of the annular Fresnel lens are listed in Table 1. Utilizing the proposed adaptive optimization solution, we obtain that the form of the backlight unit is free-form shaped as shown in Fig. 5(a). The variation of RMS among defocused spots considered in the calculation is plotted in Fig. 5(b). From the picture we can see that it has an increasing trend when the spot is far away from the optical axis. By arranging the backlight sources along the calculated free-form surface (FFS), we can achieve an optimized naked-eye 3D system as shown in Fig. 6. The view zone in this kind of naked-eye 3D display is different from that in a planar backlight based 3D system. The distance to LCD for any defocused spots formed by any point light source on the FFS backlight unit remain nearly unchanged. As a result, it will obtain higher

Table 1. The parameters of the circular Fresnel lens used in the calculation.

Parameters of the circular Fresnel lens	Value for every parameter
Material type	PMMA
Refractive index	1.49
Transmittance	92%
Focal length (mm)	185
Length (mm)	100
Width (mm)	100
Thickness (mm)	2
Tooth width (mm)	0.5

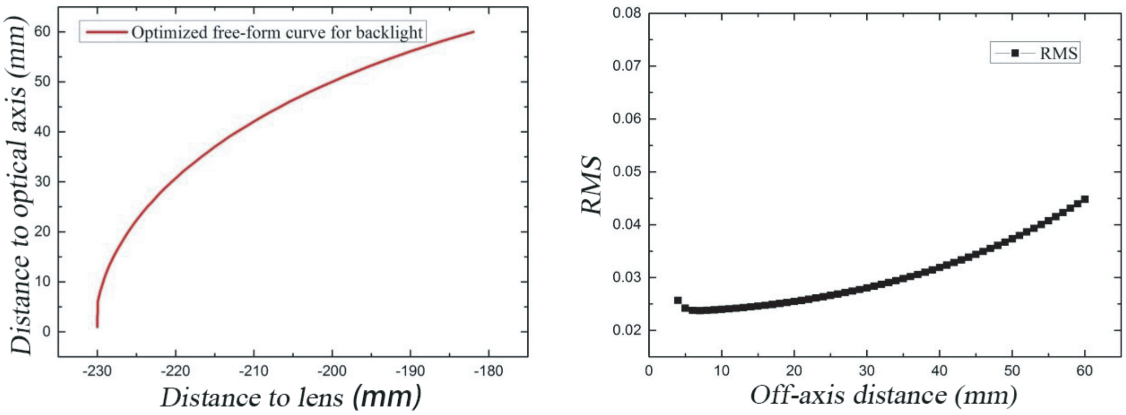

(a) (b)

Figure 5. (a) The free-form curve for arranging the backlight unit calculated by the proposed method, (b) the value of RMS of defocused spots at different off-axis distance.

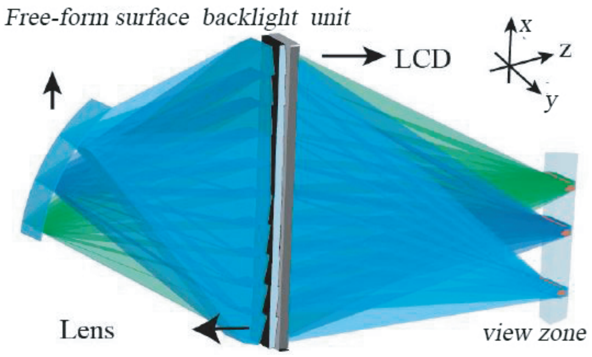

Figure 6. Top view of naked-eye 3D system based on free-form surface backlight unit, x-y plane is parallel to the LCD, z-axis is perpendicular to the LCD.

luminance homogeneity within the viewing zone, even though the viewer is moving around within the view zone.

The proposed optical design method is universal for time-spatial multiplexing naked-eye 3D display. The design for Fresnel lens or for the backlight unit can be determined if the system input, including the viewing distance, the number of total viewing zones, the dimensions of each viewing zone, the size of LCD, is specified.

2.3. Overall Design Scheme for a Single-User Naked-Eye 3D Display

According to the proposed optical design method, a two-viewing-zone naked-eye 3D display can be readily obtained. Fig. 7 shows the schematic diagram of a single-user naked-eye 3D display. In order to reduce the thickness of the system, a 3×5 circular Fresnel lens array is used as the LCE instead of a single big Fresnel lens. The size for each square-shaped circular Fresnel lens is $10 * 10\,\text{cm}^2$. The total lens array has an area of $50 * 30\,\text{cm}^2$, which is close to the size of a 23-inch LCD. The refreshing rate of the LCD is 120 Hz. Behind every lens unit, there are two light sources to alternately illuminate the corresponding area of LCD. The total backlight module can be divided into two groups (a red one and a green one with the LED array of 3×5). As shown in Fig. 7(a), the red group backlight will be turned on when the LCD is displaying the left image. On the other hand, the green group backlight will be turned on while the right-eye image is loaded on the LCD. All of the LEDs are arranged along a free-form surface calculated by the proposed adaptive optimization solution. All of the light emitting from the red or green group will be brought to the area of left or right viewing zone. There may be some leakage to the adjacent view zone, which is termed as crosstalk, can be calculated by

$$\text{Crosstalk} = \frac{L_{leakage} - L_{background}}{L_{signal} - L_{background}} \times 100\% \tag{7}$$

where $L_{leakage}$, $L_{background}$ and L_{signal} respectively denote the light intensity of leaking light, background light and signal light. It is reported that the viewer may perceive ghost image and even feel uncomfortable if the crosstalk is beyond 5% [7, 8].

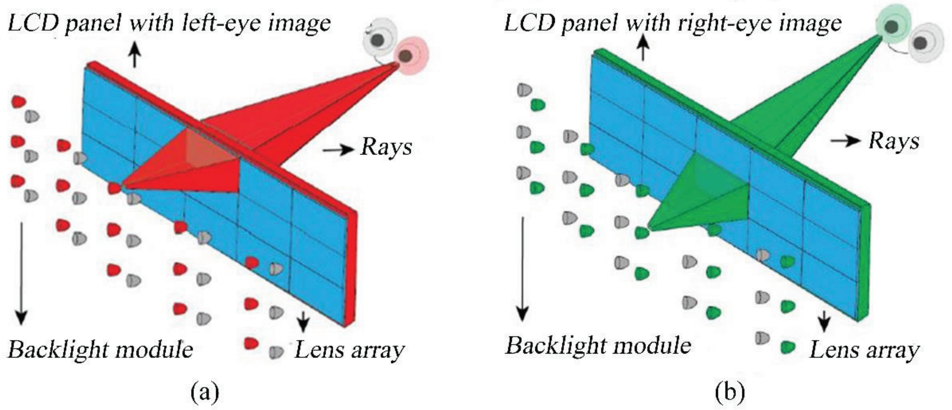

Figure 7. Schematic diagram of a single-user naked-eye 3D system (a) turning on left-viewing LEDs and (b) turning on right-viewing LEDs.

The prototype for this designed naked-eye 3D display is shown in Fig. 8(a). The interior of the prototype is also presented in the same figure. In order to improve the homogeneity of the light sources, a diffuser is placed in front of every two-LEDs as shown in the left bottom of Fig. 8(a). The LED is installed on a circuit board with a black columnar cover as shown in Fig. 8(b), to limit the emitting angle so as to reduce the crosstalk. The front view of the working prototype is shown in Fig. 8(c). The optimum viewing distance is set around 900 mm for this particular display unit. The range of freely movement for viewer(s) is greater than 100 mm in the Z direction. The luminance distribution is measured by a PR655 Spectra Scan (manufactured by Photo Research INC). The PR655 is set at the best viewing distance of 900 mm. During the measurement of the luminance of the left view zone, the left- and right-eye images are respectively set as a white picture and a back one. For the measurement of right view zone, the loading images on LCD for left and right view zones are in the contrary ways. After finishing the luminance measurement, the crosstalk ratio among the whole viewing zones can be calculated by formula (7). As shown in Fig. 9, the luminance reaches a peak value of $213\,\text{cd/m}^2$ for both viewing zones at the viewing positions of -40 cm and 40 cm. The minimum crosstalk ratio is 3.9%, which means that the viewer at this viewing position will obtain a comfortable naked-eye 3D picture or 3D video.

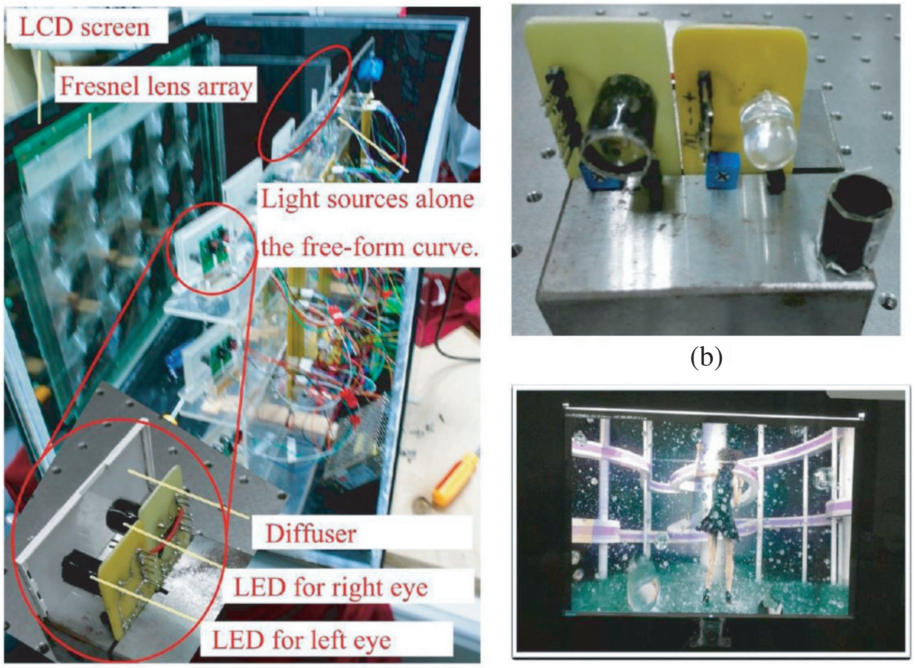

(a) (b) (c)

Figure 8. (a) The internal structure of the two-view-zone naked-eye 3D prototype, (b) the two-LED module with a black columnar cover, (c) the displaying effects of the prototype.

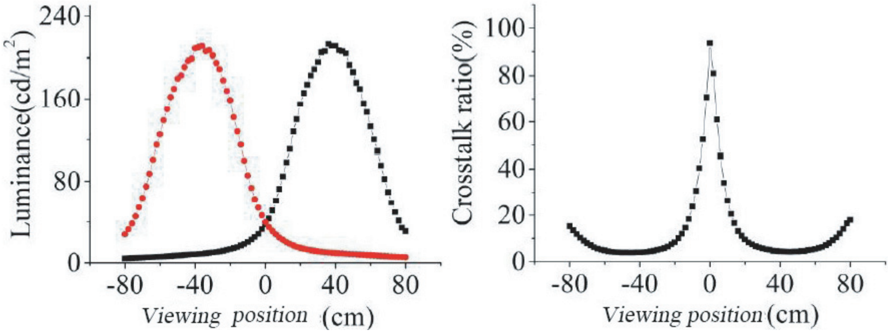

(a) (b)

Figure 9. (a) The luminance distribution and (b) crosstalk ratio of the two-view-zone prototype, among the entire view range from −80 cm to 80 cm.

2.4. Overall Design Scheme for a Multi-Viewer Naked-Eye 3D Display

In many situations, a multi-viewer naked-eye 3D display is required. For example, in a family or other public places, there will be more than one person to simultaneously watching 3D program. Hence, it is necessary to design a multi-user naked-eye 3D display.

Here we present a six-viewing-zone case as shown in Fig. 10. In order to expand the range of view zone in the y-axis (horizontal) direction, a series of LED light bars are used to constitute the backlight module in this system. The width of each view zone is set as 50 mm in the x-axis direction. Coordinates of the left and right edges of all viewing zones are marked in Fig. 10. Utilizing the proposed RMS-based adaptive optimization solution, the position of light sources can be determined. For the lens array composed of three pieces of linear Fresnel lens, three groups of backlight units are installed. Each group of backlight unit contains six light bars arranged along the calculated free-form surface. When turning on all the LED bars labeled as 1 in all backlight group, the viewer in viewing area 1 will perceive the

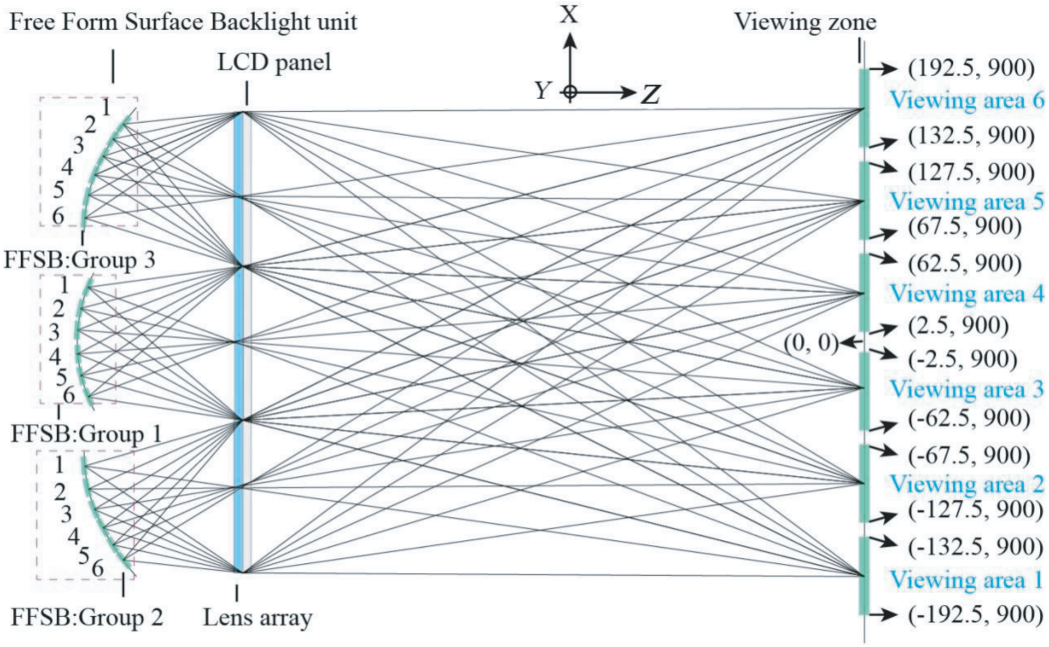

Figure 10. Top view of the schematic diagram for a six-view-zone system, x-y plane is parallel to the LCD screen, the z-axis is vertical to the screen. The origin of the coordinate system is set at the middle of LCD screen. The corresponding coordinate values of boundary points for all viewing zones are marked in this figure.

full-resolution image displaying on LCD. Other viewing zones work in a similar way.

Most importantly, this six-viewing-zone system can work in both single-user mode and multi-user mode by different control modes on the backlight module. When being used in single-user mode, the system needs to turn on any adjacent two corresponding LED bars in each backlight group, such as light bars l and 2, respectively responding the viewing areas 1 and 2. Again for instance, turning on light bars 4 and 5 in all the backlight groups, responding viewing areas 4 and 5, a person located at this pair of viewing zones will see the 3D images. When being worked in multi-user mode, the system needs to turn on four light bars in correspondence to the positions of the viewers. It is important to note that the distance between two adjacent viewers has to be taken into account for the backlight arrangement. In this system, the distance between any adjacent viewing zones is only 5 mm. Thus only viewing areas 1 and 2 for a person, 5 and 6 for another can be used for the two users. When the LCD is loaded with the left-viewing image, the light bars 1 and 5 are needed to turn on. For its next frame, the adjacent light bars 2 and 6 will be turned on when LCD is refreshed with the right-eye image. Of course, expanding the number of backlight units horizontally is able to enlarge the viewing angle which will allow more viewers to watch the naked-eye 3D display at the same time.

To verify the accuracy of this overall design scheme, a virtual simulation is demonstrated in the optical software ASAP, based on the parameters obtained in the above system. The intensity distributions along the x-y plane at the viewing distance of 900 mm are demonstrated in Fig. 11. Here x-y plane is parallel to the LCD screen, and z-axis represents the value of light intensity. The picture shows that the variation of the light intensity for each view zone along the horizontal direction (x-axis) and vertical direction (y-axis) is rather small. The viewing range in the vertical direction is bigger than that in the horizontal direction whose size is just about 50 mm. Viewing zones characteristic in horizontal direction should be treated with great care, especially for their luminance homogeneity, as the crosstalk will be introduced by the leakage light from other viewing zones. For this system, the curve of the light intensity in each view zone is nearly flat as shown in Figs. 9(c) and (d), producing a well defined homogeneity required for display.

Based on the well simulated homogeneity and low crosstalk, a prototype is built for this multi-

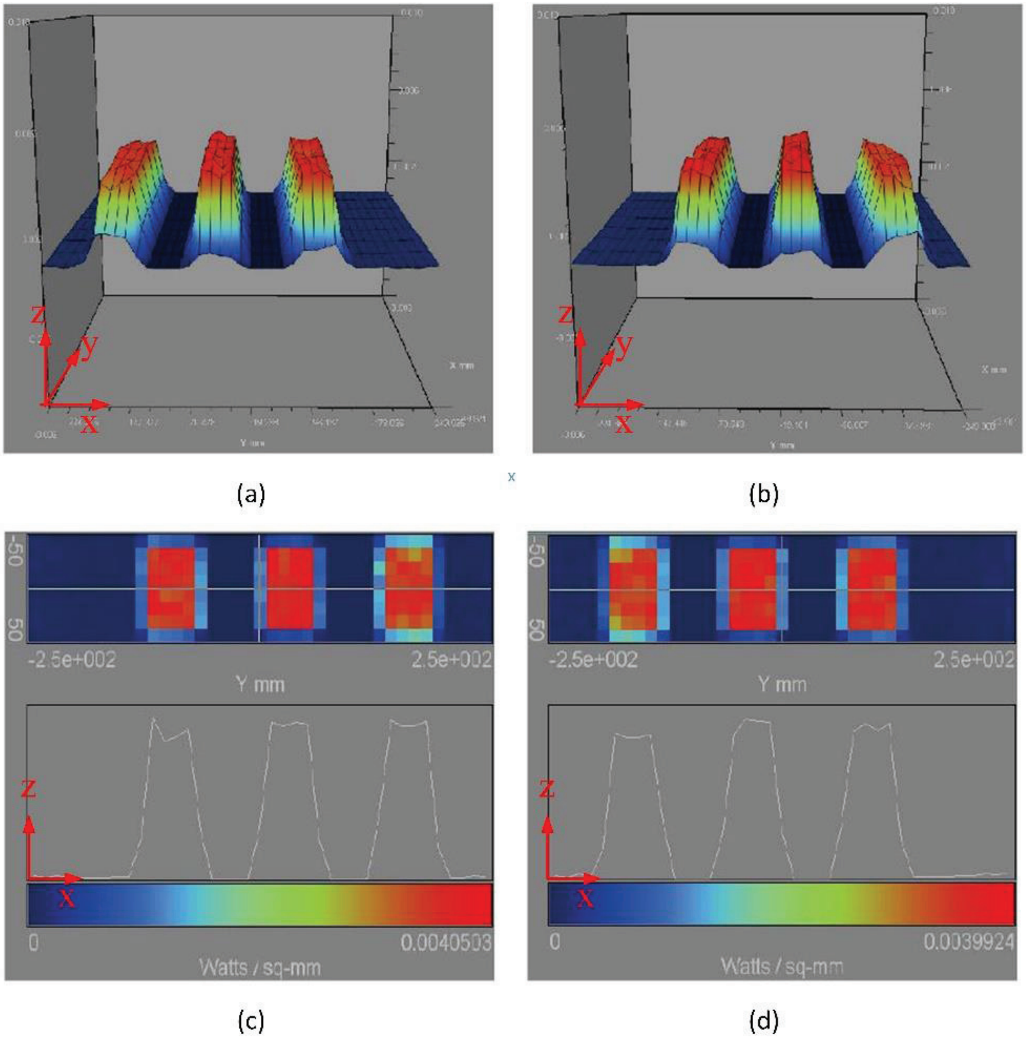

(a) (b) (c) (d)

Figure 11. Intensity distribution at the viewing plane obtained in the simulation, when turning on (a) light bar 1/3/5, (b) turning on light bar 2/4/6. And the corresponding variation of intensity along the x-axis is shown in (c) and (d).

viewing-zone system. The LED light bars are fixed along the black curve on the circuit board as shown in Fig. 12. Furthermore, there is an integrated circuit on each circuit board to turn the six LED light bars on/off. The internal structure of the prototype is shown in Fig. 13. In this prototype, a series of LEDs and diffuser are adopted to form an LED light bar which can be regarded as a rectangular surface light source as shown in the upper left of Fig. 13. The Fresnel lens array in this prototype consists of five linear Fresnel lenses. The appearance of a single linear Fresnel lens is shown in the right bottom of Fig. 13. The green and red areas on the viewing plane are shown at the right of Fig. 13, respectively corresponding to the left and right view zones. Here only two light bars behind each lens are turned on, and the image loaded on LCD is a green/red image for the left or right view zone. This plot clearly shows the directional propagation of left and right viewing images in the time-spatial multiplexing naked-eye 3D display. The viewing angle in vertical direction (y-axis) is ±9.5°, which offers a range of 30 cm in the vertical direction for a viewer to move up and down.

All of the viewing zones in this prototype are shown in Fig. 14(a). The luminance distributions among those viewing zones, measured by a spectroradiameter PR655, are shown in Fig. 14(b), which deviates from that obtained in the simulation as shown Fig. 11. The luminance distribution curve obtained in simulation has a flattop in each view zone, with a steeply rising and falling edge. However,

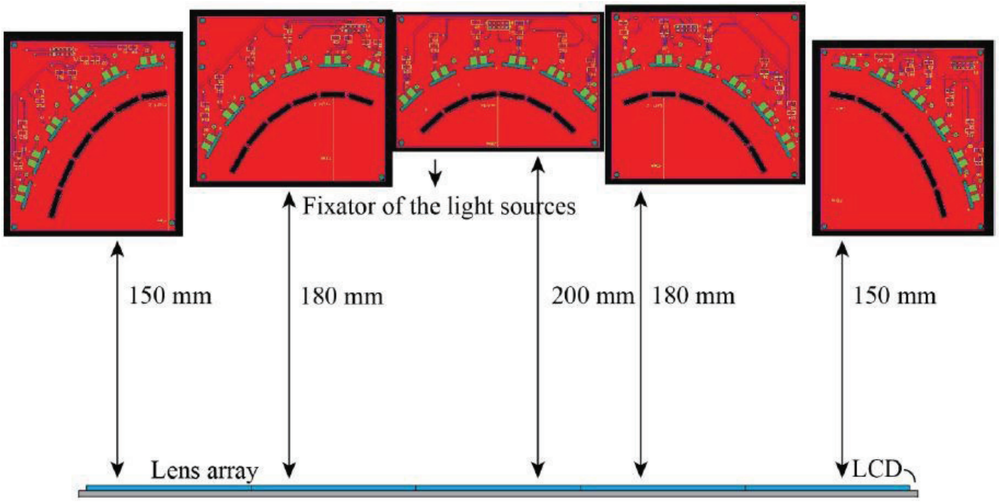

Figure 12. The schematic drawing of the free form surface backlight modules.

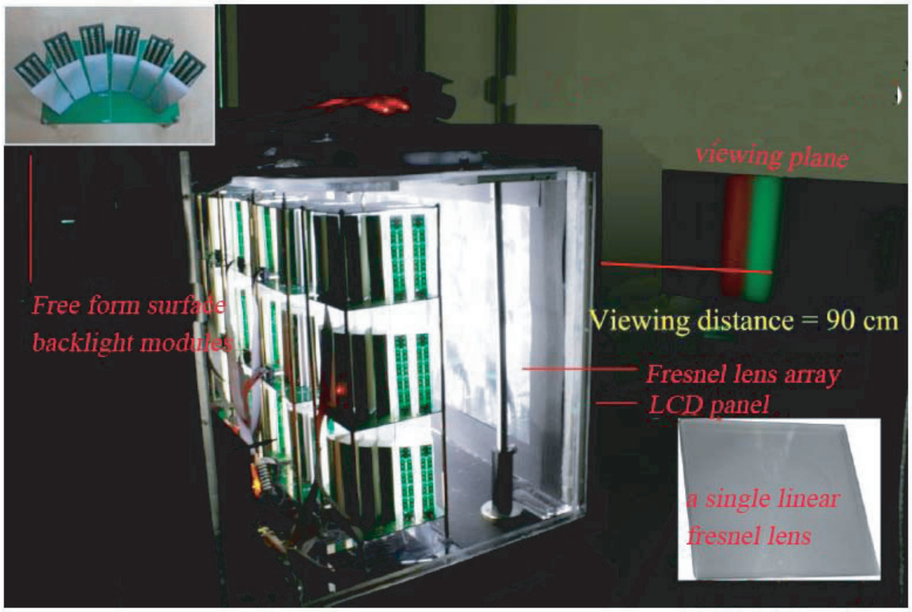

Figure 13. The internal view of the prototype and the corresponding view zones.

the brightness distribution curve for the prototype in every zone is Gaussian shaped. The reason for this can be explained by the following points. Firstly, the width for each light bar is 15 mm, which is different from the ideal size. Theoretically, the widths of light bars are different, changing within the range from 15 mm to 17.3 mm. Hence, the viewing zones formed by those off-axis light bars will be required to become narrower towards the edge. Secondly, the width of a single Fresnel lens is set as 100 mm for the design for the simulation. However, the actual size deviates from 100 mm with some unavoidable mismatching tolerance. The distances between two adjacent lenses' middle positions are respectively 98.04, 98.25, 97.53 and 98.33 mm. Therefore, the light concentrated by each lens cannot exactly reach the designed zones. Finally and most importantly, the positions of light source and lens array in the prototype are not completely coinciding with the simulation location. Thus, in order to obtain a prototype whose effect is equivalent to the simulated results, the manufacturing and assembly accuracy needs to be improved.

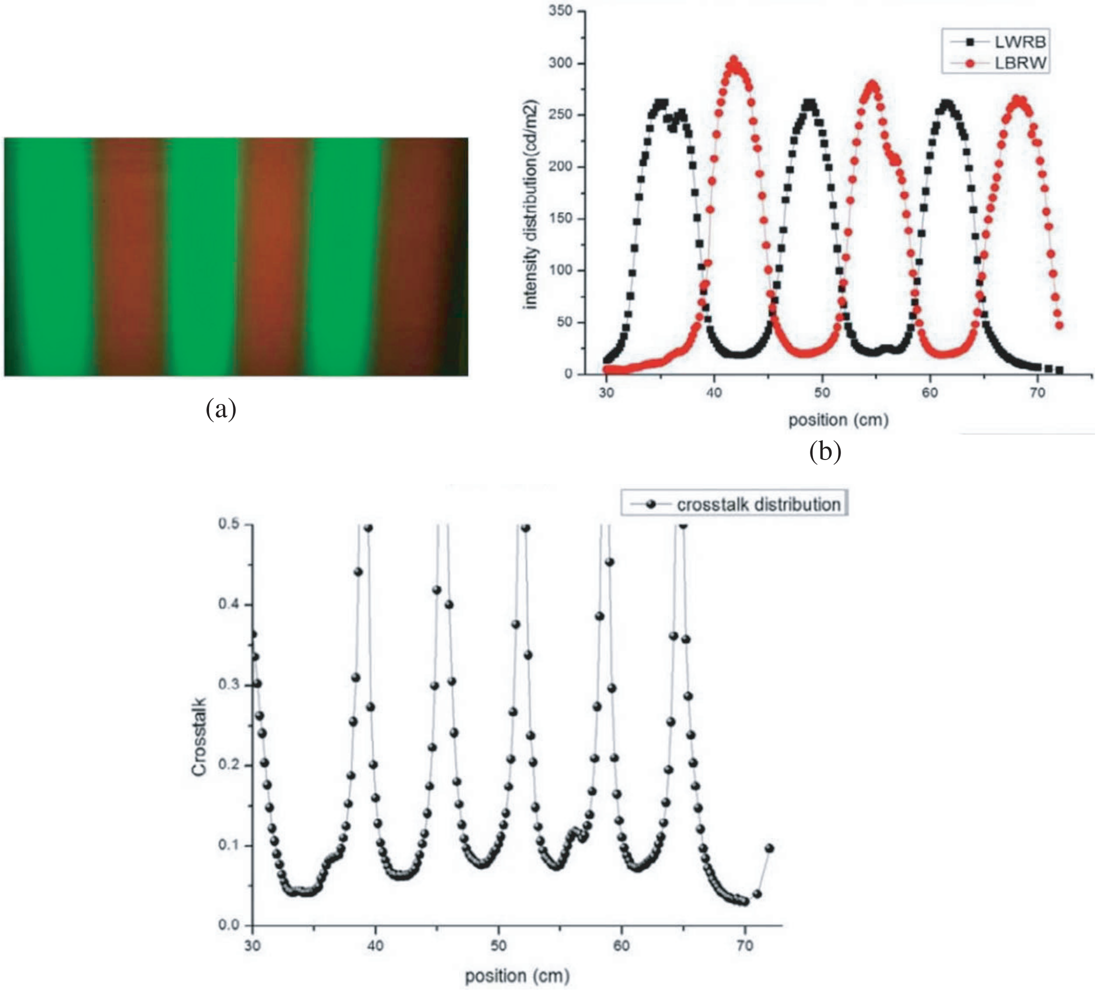

(a)

(b)

(c)

Figure 14. (a) Viewing zones, (b)intensity distribution and (c) crosstalk for the prototype.

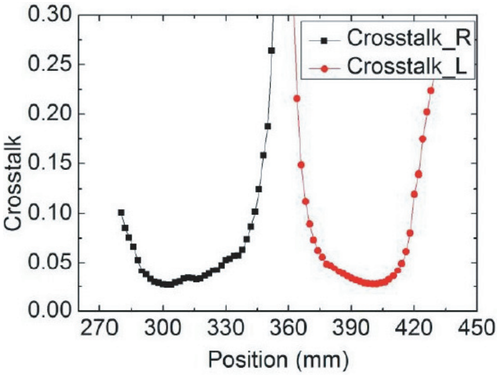

Figure 15. The crosstalk distribution for two viewing zones after employing the eye tracking technology.

The crosstalk distribution for all the viewing zones obtained by formula (7) is shown in Fig. 14(c). The crosstalk ratio for each view is less than 10%. If eye tracking technology is applied to better determine the location of the viewer, it can be reduced to less than 5%, as shown in Fig. 15. The achieved lowest crosstalk is about 2.41%, which is close to the level in the polarizer glass assisted 3D display. This value will make most viewers relatively comfortable for their watching the naked-eye 3D experience.

The images received at six viewing zones have very little difference from each other as shown in Fig. 16. The resolution in 3D mode of this prototype is the same as that in 2D mode as shown in Fig. 17. The left bottom illustrations in both pictures are obtained by a magnifying lens. Furthermore, the luminance and color gamut in NTSC have also been measured with a spectroradiameter, whose values are shown in Table 2. It is also necessary to point out that the data format of the sources used in this system is compatible with the existing shutter-glass based 3D video program, hence significantly extending its applicability.

Figure 16. The images obtained at six viewing zones of the prototype.

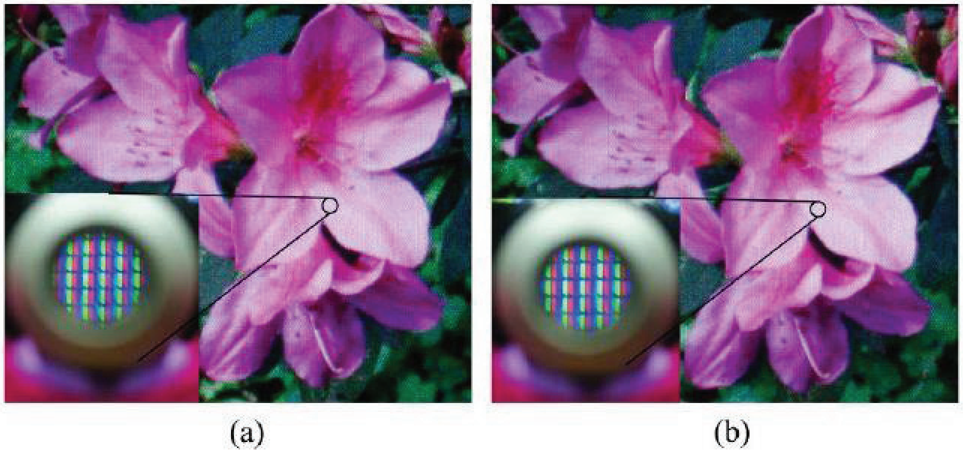

Figure 17. The comparison between images taken in (a) 2D mode and (b) 3D mode.

Table 2. The mainly parameters for the prototype.

Parameters	Value
Size of LCD	23 in
Resolution in 2D mode	1920×1080
Resolution in 3D mode	1920×1080
Lowest crosstalk	2.41%
Luminance	$304\,\mathrm{cd/m^2}$
NTSC gamut	70.6%

3. PERFORMANCE OPTIMIZATION TECHNIQUES FOR THE NAKED-EYE 3D DISPLAY

The general theories for designing the Fresnel lens and backlight module described in detail in the above sections show that either single-user or multi-user naked-eye 3D system performs well with full-resolution and low crosstalk display. The performance needs to be further improved in order to offer an even better display effect. Among all the performance parameters, crosstalk, luminance homogeneity and moiré fringe need to be treated with great care.

3.1. Optimization Techniques for Crosstalk

Crosstalk is a very crucial parameter for the naked-eye 3D display. The 3D display system may present ghosting imaging or even cause undesired visual fatigue such as nausea, eyestrain, and headaches if the crosstalk is beyond 5% [25, 26]. Thus, to achieve the crosstalk less than 5% is utterly important. Generally, the crosstalk in naked-eye 3D system can be divided into spatial crosstalk and temporal crosstalk. The spatial crosstalk, which exists in both spatial-multiplexing and time-spatial multiplexing system, is mainly related to the optical structure of a display, and it can be decreased by a systematically optimized design and an accurate assembly of all individual elements.

However, additional temporal crosstalk exists in time-spatial multiplexing naked-eye 3D display, which is caused by the persistence of the former image during the refreshing process as shown in Fig. 18, as the loading of every frame of picture will take several milliseconds by top-down style. Latterly, the whole frame image will remain on the screen for another several milliseconds. After finishing a refreshing period of about 8.33 ms with the LCD working at 120 Hz, the LCD will continue loading the next frame image. From the pictures, we can see that there will exist partial former frame image on the screen during the loading process. If all the corresponding left- or right-backlight modules are simultaneously turned on, the left/right view zone will receive partial undesired right/left image, leading to additional temporal crosstalk.

Overcoming the temporal crosstalk can be approached with two methods: one way is to change the refreshing style of LCD suggesting additional improvement with higher cost; the other way is

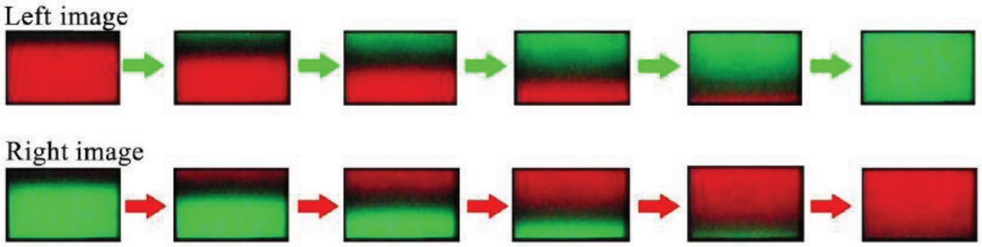

Figure 18. The refreshing process of a 120 Hz LCD captured by a high-speed camera with a frame rate of 1000 fps.

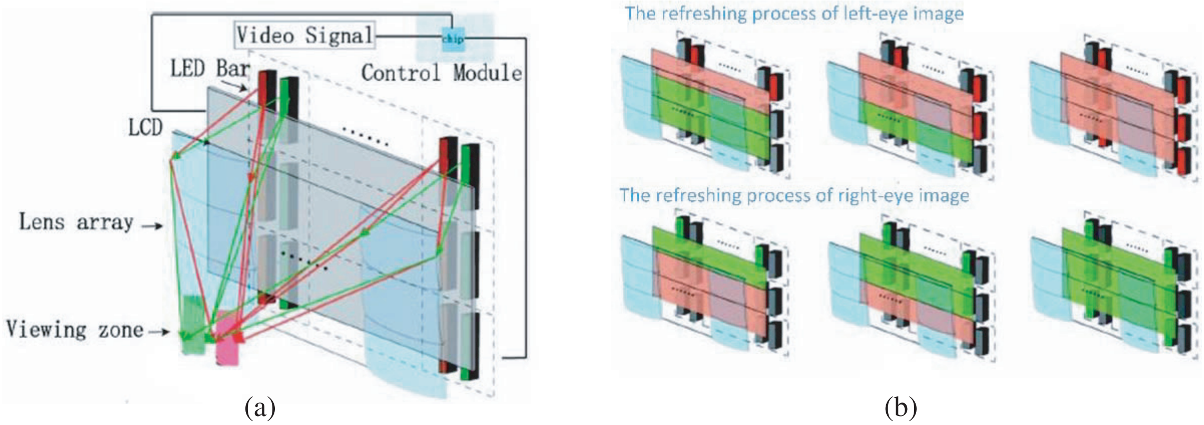

(a) (b)

Figure 19. Schematic diagram of (a) a time-spatial multiplexing naked-eye 3D display and (b) the refreshing process of dynamic synchronized backlight for left-eye image (upper) and for right-eye image (below).

to change the switching style of backlight modules. Here, the latter scheme is adopted. A new dynamic synchronized backlight technique [27, 28] is proposed and demonstrated to eliminate the temporal crosstalk. As shown in Fig. 19(a), a controller module with ICs is inserted into this system to accurately determine the switching of each LED bar to synchronize to the dynamic refreshing of LCD. In this system, the lens array is composed by 5 × 3 circular Fresnel lenses with dimensions of 100 mm × 100 mm × 3 mm. The left- and right-viewing images are dynamically synchronized with the backlight respectively, as shown in Fig. 19(b). In the picture, the red and green areas on LCD respectively represent the zones that having loaded the left- and right-viewing images. Each row of LED bars labeled in red (for left-view zone) or green (for right-view zone) will be turned on one by one with a delay time of τ, after the LCD finishes refreshing each corresponding region.

The electric signals to control the backlight bars are depicted in Fig. 20. The high levels labeled as 1 in this picture mean turning on the LED bars, while the low levels labeled as 0 mean turning off the LED bars. Triggered by the synchronizing signal for left-eye image, the first row of light bars labeled in red will be firstly turned on with a waiting time of T_W. Here the waiting time is 2 ms, which is the maintaining time of the former image. With a delay time τ to the former, the second and third row light bars will be turned on orderly. In this system, the gating time t and delay time τ need to satisfy the relation as below.

$$t + 2\tau \leq T_D - T_W \tag{8}$$

where $T_D \approx 8.33\,\text{ms}$ represents one frame time of the 120 Hz LCD. Similarly, the right-eye backlight modules are synchronized with the right-eye image.

As shown in Fig. 21, the eye in left or right-view zone will only receive the left or right-eye image in any moment. Thus, the temporal crosstalk can be effectively reduced. The crosstalk obtained within the viewing zones will differ with the gating time as shown in Fig. 22. When the gating time is beyond 4 ms, the crosstalk will rise greatly. At the gating time of 2.56 ms, it will achieve a minimum value of 2.64% for the left-view zone and 2.78% for the right-view zone. However, the lower gating time gives rise to a lower luminance for the image received in the view zones. Thus, the optimal gating time is determined by taking into account of not only the reducing of the crosstalk but also the maintaining of the comfortable luminance. Therefore, the best gating time can be set at the range of 2 ms ∼ 3 ms. Under this condition, the obtained luminance and crosstalk are respectively within the range of $200\,cd/m^2 \sim 300\,cd/m^2$ and the range of 2% ∼ 3%.

3.2. Optimization Technique for Luminance Homogeneity

It is very important to consider the luminance homogeneity, an important performance for the naked-eye 3D display. The evaluation of uniformity in naked-eye 3D is completely different from that in

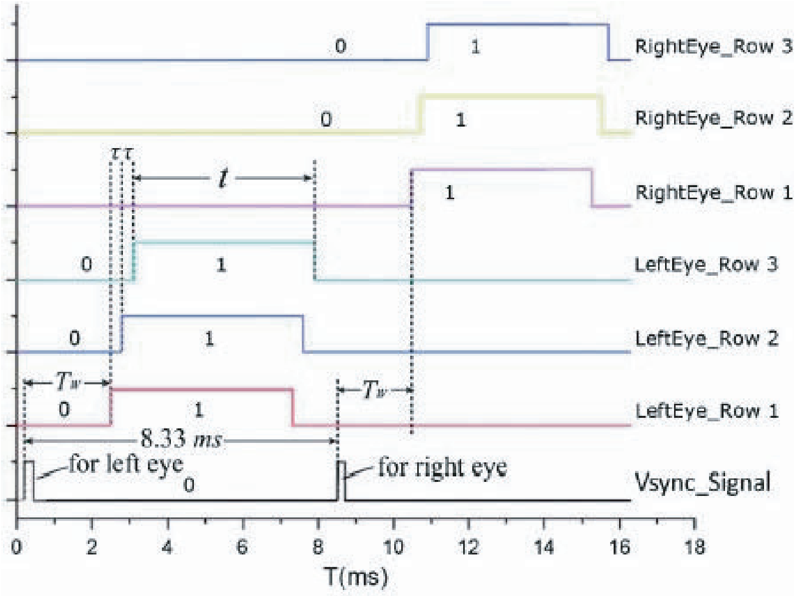

Figure 20. The timing pulse for controlling the backlight module.

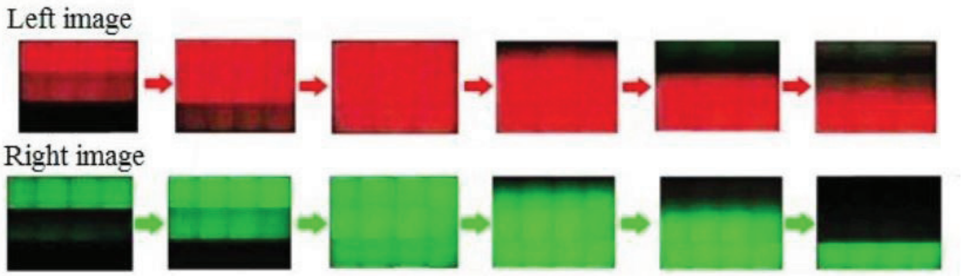

Figure 21. The displaying process of LCD based on the proposed dynamic synchronized backlight technique.

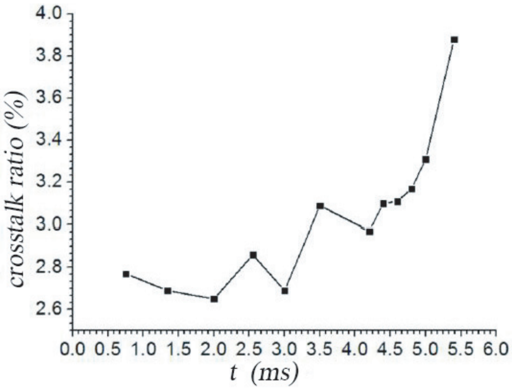

Figure 22. The relationship between crosstalk and gating time t.

conventional 2D display. For 2D display, there is an array of backlight module closely behind the LCD. The light on the LCD screen emitting from backlight module in conjunction with strong diffuser nearly subtends a 2π solid angle in the whole viewing space. However, in the proposed time-spatial multiplexing naked-eye 3D display, there are several groups of backlight units alternately illuminating the LCD to form the corresponding viewing zones. The viewing space is divided into several viewing zones with well-defined directional backlight. Only within the viewing zones, viewers can receive the image displayed on LCD. Thus the luminance homogeneity for naked-eye 3D display should be studied within the view zones for the directional backlight illumination.

In the view zones, the low luminance homogeneity on the screen received by eyes may easily occur at the joint of any two adjacent Fresnel lenses and in certain areas of the Fresnel lenses where the machining accuracy is not sufficiently accurate [29, 30]. Hence a suitable design and fabrication for the Fresnel lens are highly necessary. Furthermore, the arrangement of backlight modules may also affect the luminance homogeneity.

3.2.1. Luminance Distribution at the Joint of Lens Array

The lens array in the proposed naked-eye 3D display usually consists of several circular Fresnel lenses or linear Fresnel lenses. Ideally, the edges of two lenses should meet each other without any seam. However, there is a randomly shaped seam defect with a width of d at the joint of the adjacent lenses, as shown in Fig. 23. The seam might be introduced by the machining tolerance during the manufacturing process. In industry, the lens is made by a metal model pressing on polymer materials (such as polymethyl methacrylate). For the existing imprecision at the joint between two lenses there will exist some defects such as broken tooth, wrinkle, and coarse.

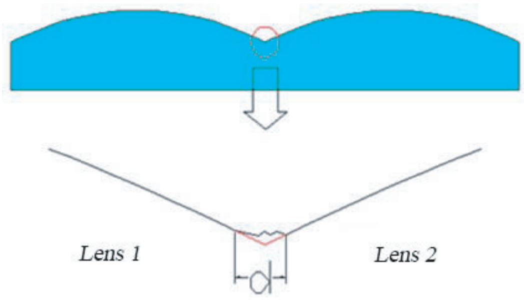

Figure 23. The seam at joint between any two lenses.

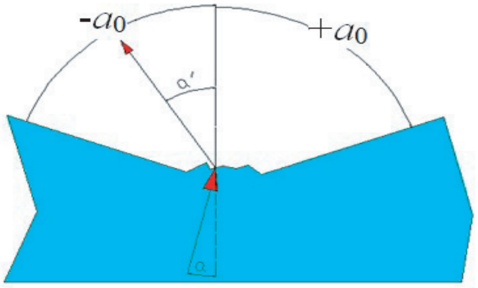

Figure 24. The random scattering model for light passing through a seam.

The light passing though the lenses will finally reach the designed viewing zones. However, light illuminating on the randomly shaped surface of the seam will exit with a random direction. Hence, we propose a randomly scattering model to analyze the behavior of light at the joint, as shown in Fig. 24. A light ray with an incidence angle of α illuminating on the seam will present a random exiting direction with an angle of $\alpha^{'}$, within the range of $-\alpha_0 \sim \alpha_0$. The possibility density function of $\alpha^{'}$ can be denoted as $p(a')$, which will satisfy the following equation set.

$$\text{Probability}\left(\alpha^{'} \in [-\theta,\theta]\right) = \int_{-\alpha_0}^{\alpha_0} p(a')da \tag{9}$$

$$p(a') \geq 0 \tag{10}$$

$$\int_{-\infty}^{+\infty} p(a')da = 1 \tag{11}$$

In the simulation, we introduce two area light sources with Lambertian luminescence property to illuminate the two lenses. After passing through the lenses, light emitting from the light sources will finally concentrate in the prismatic area labeled in red as shown in Fig. 25. The LCD is not considered in this model because it plays little role on light ray deviation. Thus the luminance homogeneity on the surface of lens array is equal to that on the LCD. In order to obtain the luminance distribution on the

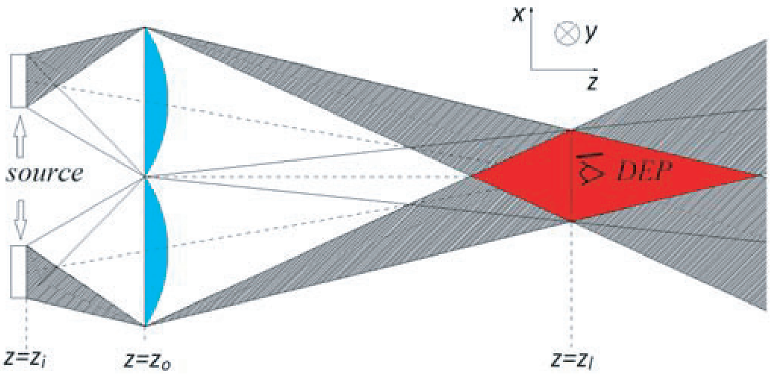

Figure 25. The light path diagram for simulating a two-lens module.

LCD received by the eye in the view zone, a small light aperture in the viewing zones with the same size of a pupil, is implanted to receive the light from the LCD. Any light entrancing this aperture may be considered as entering into the pupil. All the light illuminating on the seam will continue propagating forward by the way informed in the proposed random scattering model. However, the propagating behavior of the light illuminating on the back surface of the lenses will satisfy the Snell's law. In order to simplify the simulation, the influence of the inner structure of the Fresnel lens to the luminance distribution is unconsidered. Thus, the lens in the module is replaced by a cylindrical lens with the same concentrating function.

In the Cartesian coordinate system, a light ray emitting from the point (x_i, y_i, z_i), with an angle of θ_i to the z-axis, meets the back surface of lens at point (x_0, y_0, z_0). Thus, the direction vector of incident light can be denoted as

$$\vec{k}_i = (x_0 - x_i y_0 - y_i z_0 - z_i) \tag{12}$$

At the back surface of the lens, the light will have the first refraction. The direction vector of the refract light (denoted as $\vec{k}_r^1$) can be obtained by Equation (13).

$$\vec{k}_i \times \vec{n}_b = \vec{k}_r^1 \times \vec{n}_b \tag{13}$$

Here $\vec{n}_b$ is the unit normal vector of the lens' back surface. When the light arrives at the front surface of the lens, it will have the second refraction. Similarly, the direction vector of the existing light (labeled as $\vec{k}_r^2$) can be calculated by Equation (14).

$$\vec{k}_r^1 \times \vec{n}_f = \vec{k}_r^2 \times \vec{n}_f \tag{14}$$

where $\vec{n}_f$ is the unit normal vector of the lens' front surface.

After calculating the $\vec{k}_r^2$, the Cartesian coordinates (x_l, y_l, z_l) of the points that lights intersect the z_l-plane can be achieved. And all the all the Cartesian coordinate values are recorded into the matrix M. In order to judge whether the light entrance the pupil or not, here we import a criteria Equation (15).

$$(x_l - x_c)^2 + (y_l - y_c)^2 \leq r^2 \tag{15}$$

Here (x_c, y_c) is the central coordinate of the aperture with radius of r. The Cartesian coordinates filtered by the criterion equation are recorded in matrix $M1$.

As the minimum visual resolution is about one minute arc, the screen can be separated into a series of distinguishable units as shown in Fig. 26. Assuming that the luminous flux per unit area on LCD is N_p, the emitting direction is determined by refractive vector $\vec{k}_r^2$. The intersection angle θ_l between $\vec{k}_r^2$ and $\vec{n}_f$ can be calculated by $\cos\theta_l = \vec{k}_r^2 \cdot \vec{n}_f / \text{—}\, \vec{k}_r^2|$. The relative luminance L_r emitting from the unit area can be calculated by Eq. (16).

$$L_r = \frac{N_P}{\cos\theta_l d\Omega} \tag{16}$$

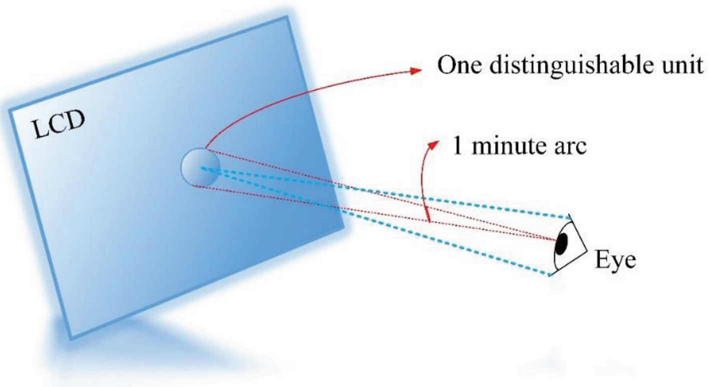

Figure 26. The diagram of human eye's distinguishable visual angle and area unit.

where $d\Omega$ is the small solid angle that the unit area subtends over the pupil. $d\Omega$ can be derived from formula (16).

$$d\Omega \approx \pi r / |\vec{k}_r|^2 \tag{17}$$

Hence, using Equations (16) and (18), the luminance of any unit area on the screen received by eye within the view zone can be obtained. The retinal illuminance is proportional to the luminance of the object and the pupil size r [31, 32]. Thus, the relative retinal illuminance (RRI) can be expressed by formula (18).

$$\mathrm{RRI} = \pi r^2 L_r \left[1 - \left(\frac{2r}{9.7} \right)^2 + (r/6.2)^2 \right] \tag{18}$$

With this equation, normalized RRI can be obtained.

Ray tracing is simulated with Monte-Carlo method. We set the size of area lightsource as $s_1 \times s_2$, the number of rays as N, the distance between lightsource and backsurface of the lens as l, the width of one lens as D, the curvature radius of the lens as c, the arc height of the lens as t, the refractive index as n, and the distance between front surface of lens and z_l-plane as L. The simulation procedure is illustrated in Fig. 27. The data used in simulation are listed in Table 3.

Table 3. Date used in the simulation.

parameter	**value**
Size of light source	0.8 mm × 2 mm
Radius of pupil	1 mm
Distance between light source to lens l	8.49 mm
Width of one lens D	4 mm
Curvature of lens c	$0.24\,\mathrm{mm}^{-1}$
Arc height of lens	3.69 mm
Viewing distance L	50 cm
Seam width d	216 µm
Number of light ray N	10,000,000

In this model, the luminance distribution at the z-plane is shown in Fig. 28(a). Ideally, in this rectangular spot, the viewer can receive the same luminance distribution on the surface of the lens array. However, only shifting within the range of $-8 \sim 8$ mm in the horizontal (x-axis) direction, the viewer cannot observe any dark band on the screen, as shown in Fig. 28(b). Thus, the luminance distribution

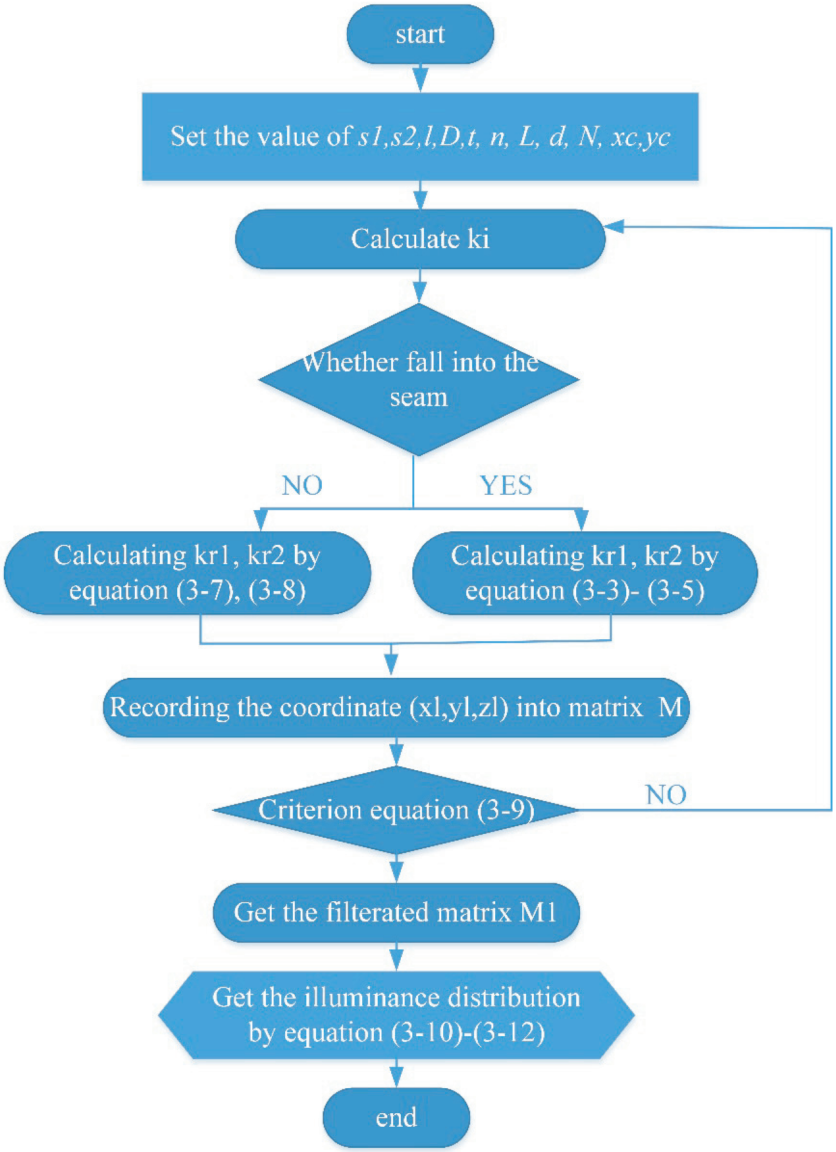

Figure 27. The simulation procedure of obtaining the illuminance distribution on the surface of lenses perceived by eye.

on the screen can be regarded as relatively homogeneous. When the viewing position is beyond 8 mm or −8 mm horizontally, a dark band will appear at the joint on the screen as shown in Figs. 28(e) to (i). The dark band will become more and more obvious with the increased horizontal shifting distance. The experimental results presented in Fig. 29 show good agreements with the simulation ones.

In conclusion, the existence of joints in the lens array may lead to the inhomogeneity of illuminance distribution on the screen when the viewer views in some areas of the viewing zone. Only within a limited range (in this simulation, it is $-8 \sim 8$ mm in the horizontal direction), the viewer can receive a relatively homogeneous luminance distribution. It indicates that the seam will reduce the view zone before the appearance of dark bands. Therefore, low luminance homogeneity caused by the seam can be improved by a better machining precision and a better design at the joint of the lens array. Furthermore, by the simulation technique proposed in this part, we can acquire the allowance machining tolerance to offer a guidance to the fabrication.

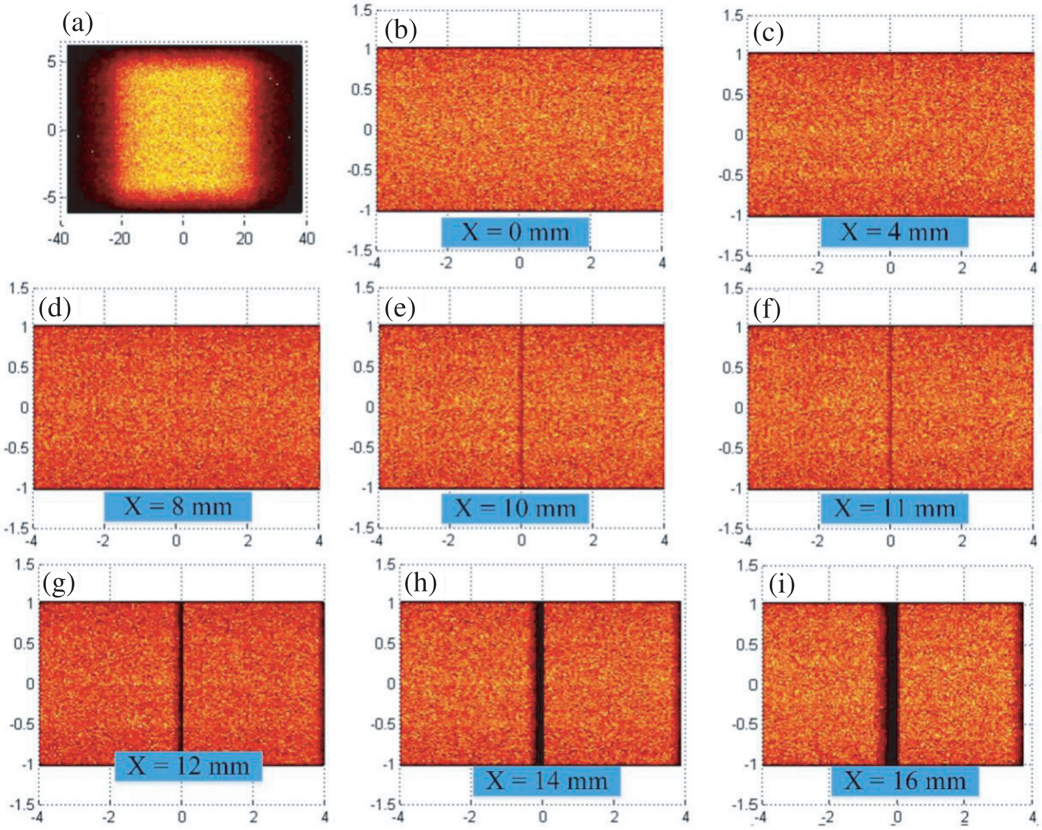

Figure 28. Simulation results. (a) The luminance distribution at the z_l-plane of the view zone obtained in the simulation, (b)–(i) the luminance distribution on the surface of two lens received by eye at different viewing position within the viewing zones.

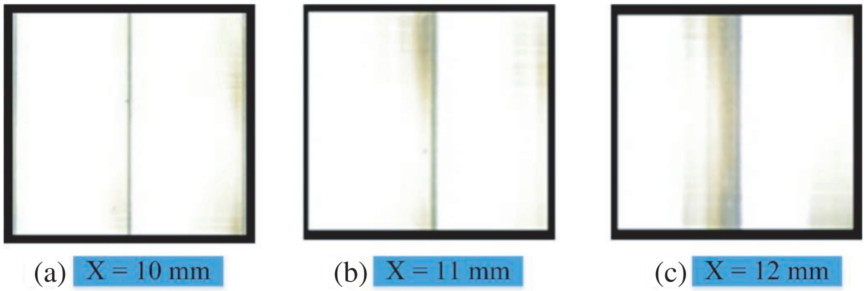

Figure 29. Experimental results obtained at different viewing positions. The luminance distribution on the screen recorded by camera respectively at the position of (a) $x = 10\,\text{mm}$, (b) $x = 11\,\text{mm}$, and (c) $x = 12\,\text{mm}$.

3.2.2. Luminance Distribution around the Central Tooth of a Fresnel Lens

In this section, the luminance distribution along a single Fresnel lens will be studied theoretically and experimentally. Fig. 30 shows the simulation model which consists of a light source and a Fresnel lens with an equal tooth depth of h. The light path is depicted in the same figure. The lens profile can be divided into three sections: the left triangular profile, central arc profile and right triangular profile, which are shaped by three diamond tools with different swivel angles. During the swap of the diamond cutting tools, the alignment may no longer be perfect, which can cause the height error between the

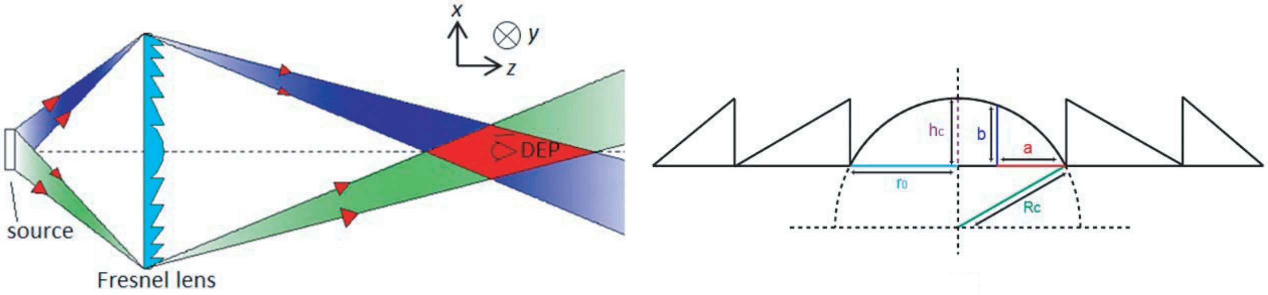

(a) (b)

Figure 30. (a) The light path diagram of a single-lens-model, (b) parameters for the central tooth of the Fresnel lens.

central arc and the adjacent triangular. To investigate the influence of radian error, the profile of center tooth is simplified as an ideal arc with a changeable radius R_c as shown in Fig. 30(b). The height h_c of the central piece and the normal vector $\vec{k}_r$ of the lens surface can be respectively calculated as follows.

$$h_c = R_c - \sqrt{R_c^2 - r_0^2} \tag{19}$$

$$\vec{k}_r = \left(\frac{X_2}{R_C} \frac{z_2 + R_C - 0.13 - h_c}{R_C} \right) \tag{20}$$

Here r_c is the half width of the central piece. Light illuminating on the lens will follow the Snell's law as described in Subsection 3.2.1. The simulation method is similar to that represented in Subsection 3.2.1. All parameters used in the simulation are listed in Table 4. For the existence of radius error, here we simulate the illumination distribution on surface of lens received by the eye located at the middle of the view zone. Subgraphs of (a)/(b)/(c) in Fig. 31 respectively represent the illumination distribution on surface of lens received by eye for the center arc height of 0 mm, 0.02 mm, 0.375 mm, while the tooth depth for side triangle pieces is 0.02 mm. From the pictures we can see that there exist dark bands in pictures (a) and (c), which may degrade the display quality of the naked-eye 3D system. In other words, the machining error of the central arc may spoil the viewing experience with the appearance of the dark bands, as shown in Fig. 31.

Table 4. The parameters used for simulation.

parameter	**value**
Size of light source	8 mm
Distance between light source to lens l	142.3 mm
Size of one Fresnel lens	10 mm
Tooth depth of lens h	0.02
Focus of one lens D	123.4 mm
Refractive index n	1.561
Viewing distance L	900 mm
Radius of pupil	2 mm
Number of light ray N	10,000,000

To verify the validity of the simulation results, two Fresnel lenses are produced as shown in Figs. 32(a) and (b). The simulative and experimental illumination distributions for lens 1 are respectively shown in Figs. 32(c) and (d), which are obtained at viewing position of (25 mm, 0, 900 mm). The distributions for lens 2 at the same viewing position are demonstrated in Figs. 32(e) and (f), showing an obviously dark band at both edges of the arc tooth. It is obvious that good agreement is obtained

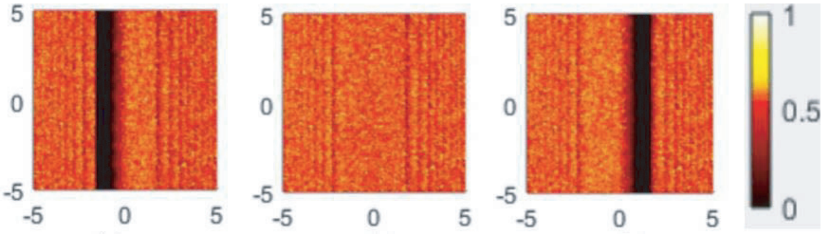

(a) (b) (c)

Figure 31. The luminance distribution on the surface of lens for (a), (b), (c) different arc height, received by eye (or camera) at the position of ($x = 25\,\text{mm}$, $y = 0$, and $z = 900\,\text{mm}$), which is in the vicinity of a boundary point of the viewing zone.

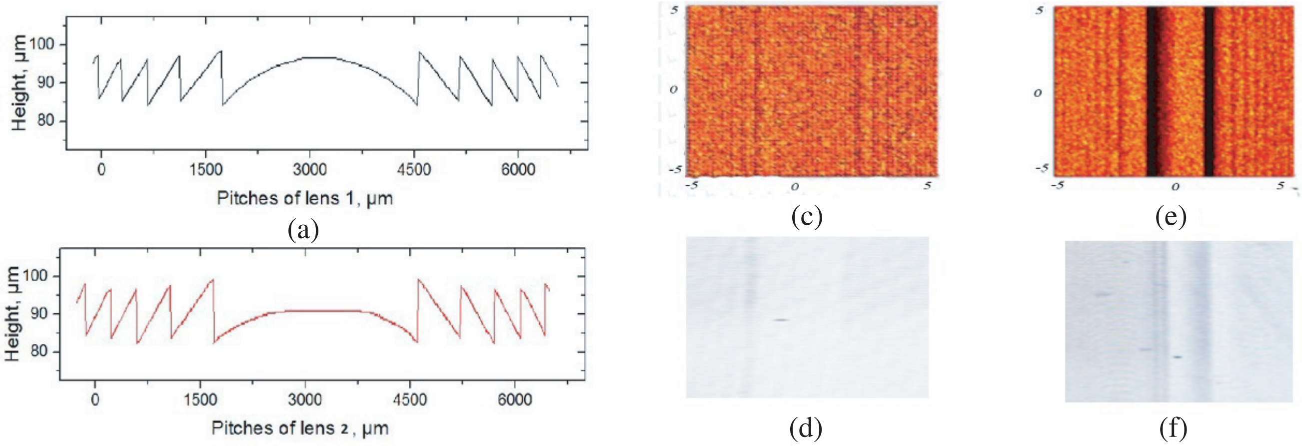

(a) (b) (c) (d) (e) (f)

Figure 32. The profile of the fabricated (a) lens 1 and (b) lens 2 obtained by a scanning electron microscope. The simulation illuminance distributions for the two lenses are shown in (c) and (e). The experimental results are shown in (d) and (f), which are received by eye or camera at the position of (25 mm, 0, 900 mm), which is in the vicinity of a boundary point of the viewing zone.

between simulated and experimental results. This further illustrates the authenticity of the simulation method used here. Hence, we can provide a guidance for the fabrication tolerance supported by the simulation results. Here the illuminance distributions of the lens for different manufacturing errors have been simulated. The relationship between the area S of the dark band and different arc heights h_c is shown in Fig. 33. From the graph, we can see that there is a flat bottom on this curve. That is to say, only in the profile of central pieces close to an ideal circular arc (where h_c is within the range of $0.013 \sim 0.025\,\text{mm}$, and R_c is within the range of $53.36 \sim 102.6\,\text{mm}$.) the dark band will be nearly invisible.

Furthermore, it is found that the appearance of the dark band is viewing position dependent. When a viewer is located closer to the center of the viewing zone, such as point of (10 mm, 0, 900 mm), a uniform image will be perceived. Here the viewing zone free from dark band is studied both numerically and experimentally for lens 2. The viewing distance in z-axis is from 800 mm to 1000 mm, which is in the so-called comfortable viewing zone. In order to describe the view zone free from dark band on the LCD screen, here a half width of viewing zone in horizontal direction (x-axis) is defined. The simulated and experimental results for a series of viewing distance are plotted in Fig. 34 by black box and red circle. The black line is the linear fit of the simulation results. From the figure, we can see that there is a linear relationship between the half width of the viewing zone and the viewing distance. Only within the comfortable viewing zone as shown with shadow in Fig. 34, the viewer will perceive relatively homogeneous illuminance distribution on the screen with invisible dark band.

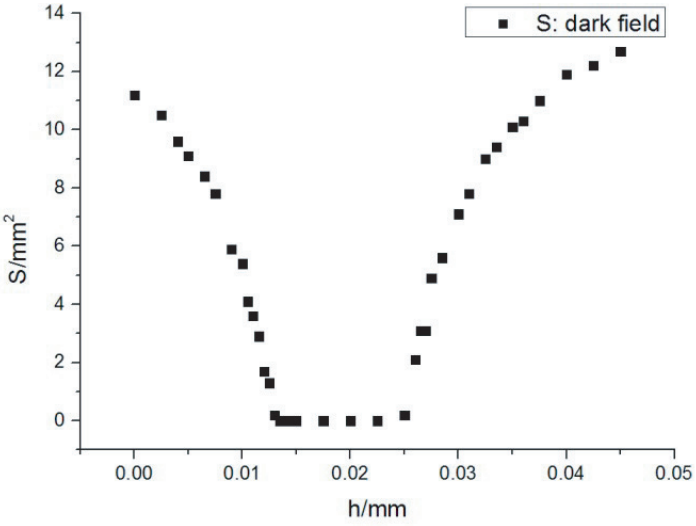

Figure 33. The relationship between the area of the dark band and central piece's arc height, while the viewer locating at the boundary point (25 mm, 0, 900 mm) of the viewing zone.

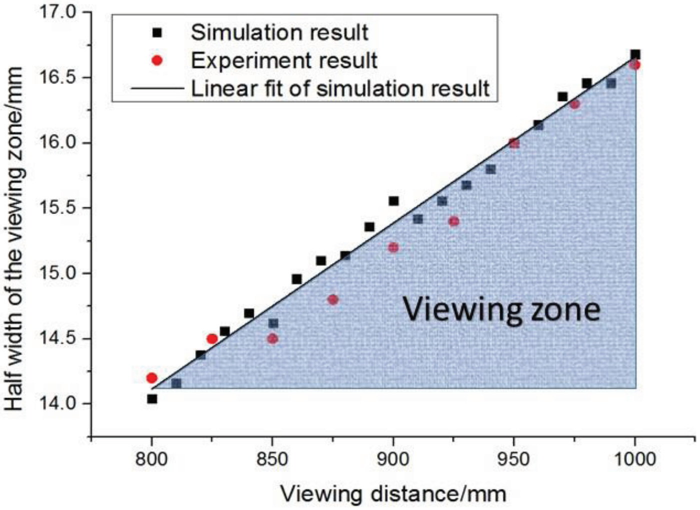

Figure 34. The half width of the viewing zone that free from dark band vary with the viewing distance.

3.2.3. Optimization for Luminance Homogeneity

Luminance homogeneity is so important for display that any dark bands on the screen should be eliminated. Any display defects, appearing either at the joints of lens array or at the central pieces of a Fresnel lens caused by the machining error, will degrade the viewer's viewing experience drastically. One of the solutions is then to control the fabrication process of the lens as precisely as possible so as to minimize the machining error. However, this error cannot be totally eliminated. Even though a dark band in the so-called comfortable viewing zone could be avoided, the half width of the view zone is still a limit as it is not sufficiently large for a viewer to move around. In other words, the viewing freedom in the horizontal direction is so small that the viewer cannot move freely. Otherwise, some display defects may appear in the viewer's eye. As the dark band perceived by the eye is mainly caused by the manufacturing deficiency at the joint of lens array or the central pieces of Fresnel lens, the viewing area is nevertheless limited. Thus, an alternative solution is to redesign the backlight system to compensate the imperfection, so that the dark bands or other displaying defects on the screen can be completely invisible, even with existing fabrication defects on the lens array. By broadening the width of viewing zone in the horizontal direction, the viewer can move with greater freedom.

Here we design a continuous backlight system as shown in Fig. 35. The backlight module for one lens is composed by several narrower light bars, which are placed behind the lens along a free-form surface calculated by the method proposed in Subsection 2.2. In the traditional one-light-bar corresponding to one-view-zone mode, the view zone's position is fixed. However, the viewing zone in the continuous backlight system can shift along the horizontal direction just depending on the position of viewer's eye by selectively turning on the corresponding backlight bars. For example, when light bars B and C are turned on simultaneously, the eye located at middle point (labeled as L) of the viewing zone illuminated by these two light bars will perceive a uniform illumination on the screen. When the eye moving away from the middle point of the view zone formed by light bar B, to the boundary position (labeled as L') of this view zone, a dark band will occur as discussed above, as shown in Fig. 35(b). In this case, if light bar A is turned on, and meanwhile turning off light bar C (to avoid the waste of luminous energy and undesired crosstalk), the eye at the same position of L' will no longer perceive the dark bands.

3.3. Optimization for MoirÉ Pattern

The displaying quality of a display system can also be degraded by the appearance of moiré pattern [33–35]. In the proposed time-spatial multiplexing naked-eye 3D display, there is two periodic or quasi-periodic optical devices, the LCD and the Fresnel lens array, with the comparative spatial periods at sub-micrometer range, where moiré pattern may easily emerge. One way to eliminate the moiré pattern is to reasonably arrange the gating periods and intersection angles among these gatings, so that it cannot be recognized by a human eye. However, changing the period of the functional optical devices such as

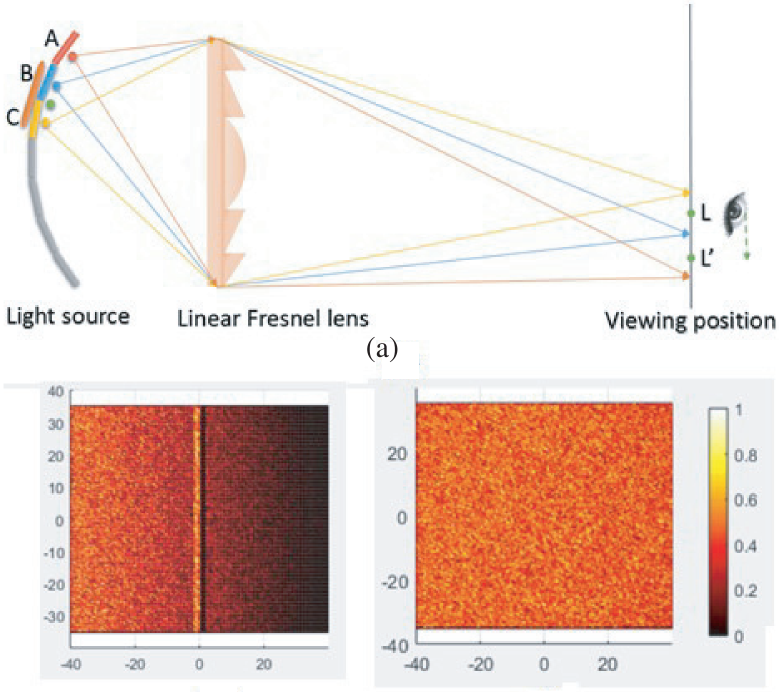

(a)

(b)

(c)

Figure 35. (a) The diagram of continuous backlight system whose light bars is placed along a free-form surface, and the viewing zone is unfixed by alternately turning on the light bars, (b) illuminance distribution on the screen obtained by eye at the boundary position of the viewing zone formed by light bar B when turning on light bar B&C, (d) illuminance distribution at the same position when turning off light bar C and turning on A.

Fresnel lens array may mean alter itself function as a light concentrating equipment. Furthermore, the display effect may be substantially degraded when the intersection angle around or greater than 10 degree. Another method is to insert a low-pass filter to weaken the intensity of moiré pattern, which will make the display system costly and bulky. There have been few reports about how to quantitatively judge whether the moiré pattern can be visible or not. Firstly, we proposed a quantitative evaluation mechanism for the moiré pattern based on the Fourier analysis method [36] combining with the contrast sensitivity function (CSF) to evaluate the value of contrast sensitivity of moiré pattern produced in a two-binary-grating mode. We then propose a novel pseudo-random arranged sub-pixel array to reduce the visibility of moiré pattern [37].

The CSF recorded as $s(f)$ describes the relationship between spatial frequency of the object and the visual sensitivity, which can be expressed by Equation (21).

$$s(f) = \frac{1}{m_t(f)} = \frac{M_{opt}(f)/g}{\sqrt{\frac{2}{T}\left(\frac{1}{X_0^2} + \frac{1}{X_{\max}^2} + \frac{1}{N_{\max}^2}\right)\left(\frac{1}{\eta p E} + \frac{\phi_0}{1 - e^{-(f/f_0)^2}}\right)}} \tag{21}$$

where $M_{opt}(f)$ is the optical modulation transfer function for human eye, which can be calculated by the formula (22), σ is the standard deviation of linear scaling function.

$$M_{opt}(f) = e^{-2\pi^2\sigma^2 f^2} \tag{22}$$

Here E represents the light intensity on the retina, which can be calculated by formula (23), where L is the average light intensity on the grating. d denotes the diameter of the pupil, which can be calculated by formula (23).

$$\begin{gathered} E = \frac{\pi d^2}{4} L \left\{1 - (d/9.7)^2 + (d/12.4)^4\right\} \\ d = 5 - 3\tanh\left\{0.4 \log\left(L X_0^2/40^2\right)\right\} \end{gathered} \tag{23}$$

The meaning of other parameters in the CSF are listed in Table 5.

Table 5. The parameters used in the CSF and the corresponding physical implications.

Parameters	Meaning
$\mathbf{m_t(f)}$	Contrast sensitivity threshold function
$\mathbf{g}$	Signal to noise ratio
$\mathbf{T}$	Integral time of human eye
$\mathbf{X_{max}}$	Largest viewing angle of human eye
$\mathbf{N_{max}}$	Biggest integral number of cycles
$\boldsymbol{\eta}$	Quantum efficiency of human eye
$\mathbf{p}$	Photon conversion factor
$\boldsymbol{\phi_0}$	Spectral density of lateral nerves noise
$\mathbf{f_0}$	Spatial frequency of lateral inhibition ceases

The curve of CSF can be obtained by Equations (21)–(23), as shown in Fig. 36, which shows that the value of contrast sensitivity will fleetly increase with increasing spatial frequency. After reaching a peak value at the spatial frequency of 3 cyc/degree, the contrast sensitivity will gradually decline. The human eye is most sensitive to green light with wavelength of 546.1 nm, but the contrast sensitivity difference for different light wavelengths is very small [38]. Thus, the colorful moiré pattern can be treated as a monochromatic one. When the spatial frequency is beyond 55 cyc/degree, the value of contrast sensitivity will be less than 1. In other words, the picture contrast, calculated by ratio of minimum to maximum light intensity, is beyond 1, which has no physical interpretation. Thus, the colorful moiré pattern can be regarded as the cutoff spatial frequency beyond which the human eye cannot distinguish the details of the objects.

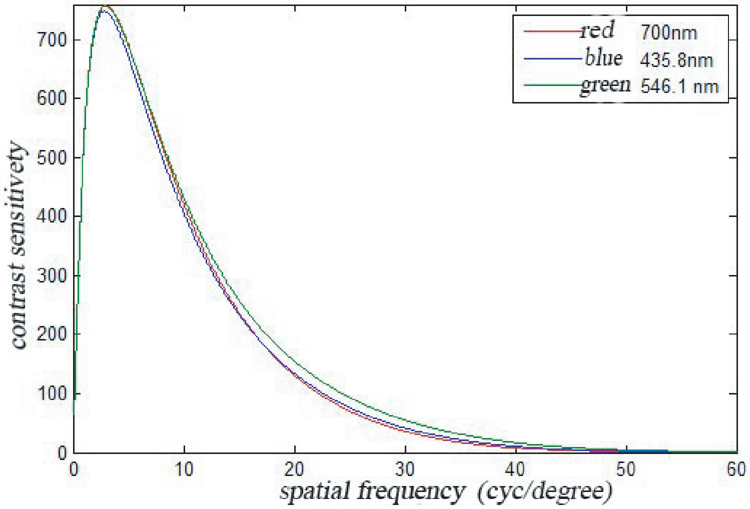

Figure 36. The curve of CSF for the red/blue/green light. The values of the parameters are set as below: $g = 3.0$, $T = 0.1\,\text{sec}$, $\eta = 0.03$, $X_{\max} = 12^\circ$, $\emptyset = 3 \times 10^{-8}\,\text{secdeg}^2$, $\sigma = 0.525\text{arc min}$, $N_{\max} = 15\,\text{cycles}$, $f_0 = 7\,\text{cycles/deg}$, $p = 1.179 \times 106\,\text{photons/sec/deg}^2/\text{Td}$, $L = 500\,\text{cd/m}^2$.

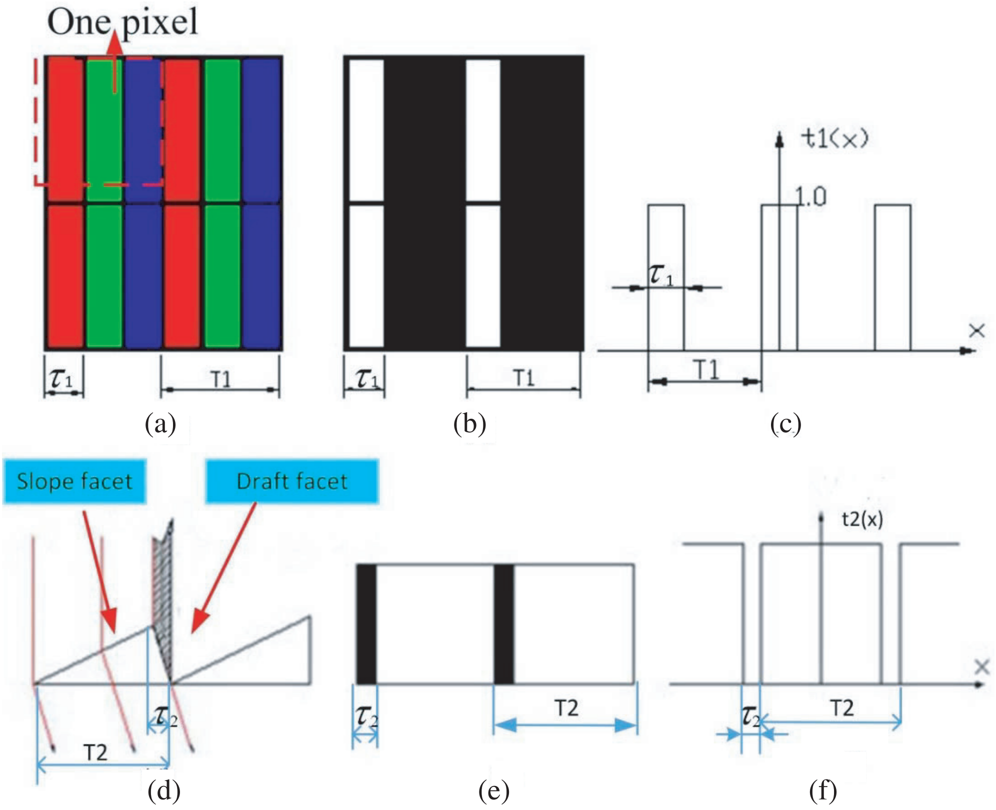

Figure 37. (a) The four-pixel structure of LCD, (b) the equivalent gating for red sub-pixel, (c) the transmittance function of the equivalent gating of red sub-pixel, (d) the two-pitch structure of Fresnel lens, (e) the equipment gating of this Fresnel lens, (f) the transmittance function of the equipment gating of the Fresnel lens.

In the proposed naked-eye 3D display system, the moiré pattern is produced by the superposition of the LCD and the Fresnel lens. Each pixel of LCD can be divided into three sub-pixels (red, green and blue, RGB) which have the same period as shown in Fig. 37(a). Since the moiré pattern is essentially generated by the interference effects, it will only happen for the light rays that have the same central wavelength. Hence, monochromatic contribution to moiré pattern is analyzed first, and the tri-color generated moiré pattern can be acquired by combining their contributions to form the polychromatic one. Thus, the LCD can be simulated as a 1-fold binary grating for each color of sub-pixel. Fig. 37(b) shows the equivalent grating of red sub-pixels with opening ratio of $\tau_1/T_1 = 1/3$. Its normalized transmittance function is shown in Fig. 37(c), which is denoted as $t_{1,R}(x)$. For the green and blue sub-pixel arrays, their normalized transmittance functions can be respectively expressed as $t_{1,G}(x)$ and $t_{1,B}(x)$. On the front surface of the Fresnel lens, there is a slope facet and a draft facet for each tooth. Ideally, the draft facet should be vertical to the flat surface (back surface). In reality, it is inevitable for the draft face that there will be a slant angle to the flat surface of the Fresnel lens as shown in Fig. 37(d). Light illuminating on the draft facet will be scattered off and perceived as dark. This part on the draft

R	1	2	1	1	1	2	1	1	3	2	1	1	3	3	1	3	2	1	3	1
G	2	1	2	2	2	1	2	3	1	1	2	3	2	1	3	1	3	3	1	2
B	3	3	3	3	3	3	3	2	2	3	3	2	1	2	2	2	1	2	2	3

(a)

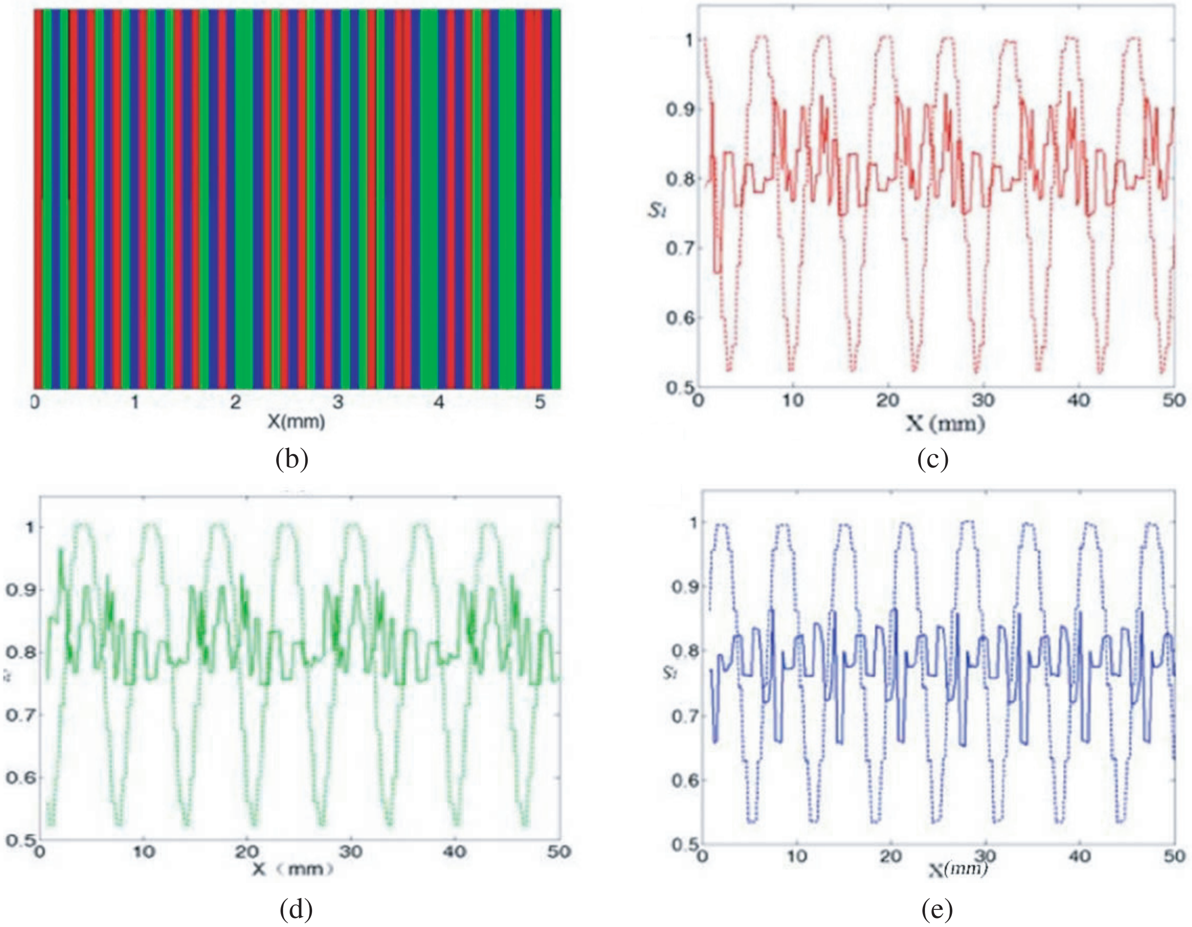

(b) (c)

(d) (e)

Figure 38. (a) The optimum randomized sub-pixel position and (b) the arrangement diagram for the first 20 pixels. The responding average intensity distribution for each color sub-pixel's equivalent grating.

facet can be considered as a barrier for light. Therefore, the Fresnel lens can be equivalent to a binary gating with the opening ratio of τ_2/T_2, as shown in Fig. 37(e). Its normalized transmittance function is shown in Fig. 37(f), and it can be expressed as $t_2(x)$. When two gratings are superimposed, the total transmittance function $t_i(x)$ can be achieved by the product of $t_{1,i}(x)$ and $t_2(x)$, where i represents different colors ($i =$R,G,B).

$$t_i\left(x\right) = t_{1,i}(x) \cdot t_2(x) \tag{24}$$

The average intensity of moiré patter can be calculated by formula (25), where $\eta\left(1, 2, 3\ldots\right)$ describes the number of grating cycles for LCD. $s_i(x)$ is the average intensity of each color moiré pattern at the length range of ηT_1 at the position of x.

$$s_i\left(x\right) = \frac{1}{\eta T_1}\int_{x-\eta T_1/2}^{x+\eta T_1/2} t_i\left(x'\right) dx' \tag{25}$$

Thus, the contrast of the color moiré pattern is given by:

$$m\left(x\right) = \frac{\max\left(s_i\left(x\right)\right) - \min(s_i\left(x\right))}{\max\left(s_i\left(x\right)\right)} \tag{26}$$

In order to eliminate the moiré pattern, the target is to obtain a minimum contrast. Thus the sub-pixels for the whole screen should be rearranged, and there are six possibilities (RGB, RBG, GRB, GBR, BRG, BGR) of rearranging the sub-pixels. In simulation, enumeration algorithm is introduced to find the smallest among all the sub-pixel arrangements. Fig. 38(a) shows the optimized position for each color sub-pixel for the first 20 pixels. Based on the optimized position, the appearance of the rearranged pixels of LCD is shown in Fig. 38(b). After the equivalent binary grating of Fresnel lens array as shown in Fig. 20(e) overlaying on the rearranged LCD, the color moiré pattern will be obtained. The average intensity distributions for the colors (R/G/B) moiré are respectively shown in Figs. 38(c), (d) and (e). The dotted-line curve and solid-line curve respectively represent the intensity distributions of moiré patterns of the original arrangement and rearrangement. For the rearranged one,

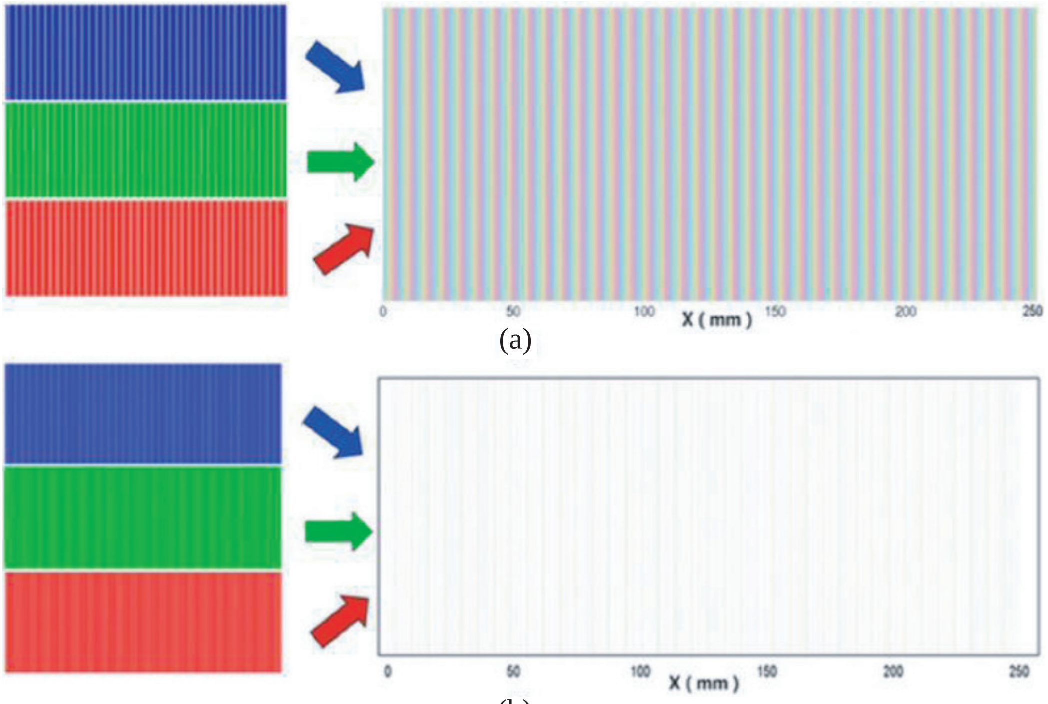

(a)

(b)

Figure 39. Visual effect of superposing of the equipment grating of LCD and Fresnel lens, (a) the original RGB arrangement, (b) the optimum RGB arrangement.

it is a pseudo-random distribution, which is entirely different from that of a conventional arrangement whose intensity distribution can be approximated as a cosine mode. Within a period, the optimum RGB arrangement disrupts the continuous variation of the original one and makes the peak of the original one disrupt into several peaks and valleys. The vibration amplitude of moiré pattern intensity for the optimum arrangement is much smaller than the original one. For the red moire pattern, the peak to peak value for the optimum arrangement is 20%, and that for the blue moiré pattern is 25%.

The visual effects of the superposing of the LCD and Fresnel lens for the original RGB arrangement and optimum RGB arrangement are respectively shown in Figs. 39(a) and (b). From the figure, we can see that the moiré pattern is eliminated by the optimization technique by rearranging each color sub-pixel. The size of the sub-pixel of LCD is about 0.8 mm. However, the wavelength of the backlight for LCD is within the visible spectrum (390 nm–780 nm). According to the optical diffraction criterion that the size of seam or hole must be comparable to that of the light wave, diffraction phenomenon is not serious, especially for illumination with incoherent light. Thus, the LCD diffraction is not taken into account.

4. CONCLUSION

In this paper, we systematically introduce a theoretical method for designing Fresnel lens and directional backlight modules. Secondly, the overall design schemes for single-user and for multi-user time-spatial multiplexing naked-eye 3D display systems are proposed and demonstrated based on the calculated free-form surface illumination technique. Finally, the performance optimization techniques about the crosstalk, luminance homogeneity, and moiré pattern are presented. Based on all the technologies mentioned in this work, a full-resolution (1080P), low crosstalk ($< 4\%$), wide viewing angle ($+-15^\circ$), high luminance homogeneity naked-eye 3D display has been achieved. Furthermore, the method described in this paper can be used as a general design guideline for the naked-eye system to achieve glassless 3D display with the highest quality for broad application purposes including virtual and augmented realities.

ACKNOWLEDGMENT

This work is supported by the National Basic Research Program of China (2012CB921904) and by the National Natural Science Foundation of China (11534017, 61505265), Pilot Project of SYSU-CMU Shunde International Joint Research Institute (20150101), and Guangdong Provincial Scientific Research Starting Foundation for Doctors (2015A030310388).

REFERENCES

1. Dodgson, N. A., "Autostereoscopic 3D displays," *Computer*, Vol. 38, No. 8, 31–36, 2005.
2. Konrad, J. and M. Halle, "3-D displays and signal processing," *IEEE Signal Process. Mag.*, Vol. 24, No. 6, 97–111, 2007.
3. Ferroli, P., G. Tringali, F. Acerbi, et al., "Advanced 3-dimensional planning in neurosurgery," Vol. 72, No. 1, 54–62, 2013.
4. Lucente, M., "Interactive three-dimensional holographic displays: Seeing the future in depth," *Acm Siggraph Computer Graphics*, Vol. 31, No. 2, 63–67, 1997.
5. Ta, S., P. A. Blanche, R. Voorakaranam, et al., "An updatable holographic three-dimension," *Nature*, Vol. 451, No. 7179, 694–8, 2008.
6. Wan, W., W. Qiao, W. Huang, et al., "Multiview holographic 3D dynamic display by combining a nano-grating patterned phase plate and LCD," *Optics Express*, Vol. 2, No. 2, 1114, 2017.
7. Ney, D. R., E. K. Fishman, and D. Magid, "Three-dimensional volumetric display of CT data: Effect of scan parameters upon image quality," *Journal of Computer Assisted Tomography*, Vol. 15, No. 15, 875–885, 1991.

8. Blundell, B. G. and A. J. Schwarz, "The classification of volumetric display systems: Characteristics and predictability of the image space," *IEEE Transactions on Visualization & Computer Graphics*, Vol. 8, No. 1, 66–75, 2002.
9. Kumagai, K., D. Suzuki, S. Hasegawa, et al., "Volumetric display with holographic parallel optical access and multilayer fluorescent screen," *Optics Letters*, Vol. 40, No. 14, 3356–9, 2015.
10. Dodgson, N. A., "Analysis of the viewing zone of the Cambridge autostereoscopic display," *Applied Optics*, Vol. 35, No. 10, 1705–10, 1996.
11. Matusik, W. and H. Pfister, "3D TV: A scalable system for real-time acquisition, transmission, and autostereoscopic display of dynamic scenes," *Acm Transactions on Graphics*, Vol. 23, No. 3, 814–824, 2004.
12. Urey, H., K. V. Chellappan, E. Erden, et al., "State of the art in stereoscopic and autostereoscopic displays," *Proceedings of the IEEE*, Vol. 99, No. 4, 540–555, 2011.
13. Liou, J. C. and F. H. Chen, "Design and fabrication of optical system for time-multiplex autostereoscopic display," *Optics Express*, Vol. 19, No. 12, 11007–17, 2011.
14. Zeng, X. Y., X. T. Zhou, T. L. Guo, et al., "Crosstalk reduction in large-scale autostereoscopic 3D-LED display based on black-stripe occupation ratio," *Optics Communications*, Vol. 389, 159–164, 2017.
15. Chen, D., X. Sang, and X. Yu, "Improved halftoning method for autostereoscopic display based on float grid-division multiplexing," *Optics Express*, Vol. 24, No. 16, 18114, 2016.
16. Allison, R. S., B. J. Rogers, and M. F. Bradshaw, "Geometric and induced effects in binocular stereopsis and motion parallax," *Vision Research*, Vol. 43, No. 17, 1879–1893, 2003.
17. Donaldson, J. K., A. J. Weinberger, J. Gagné, et al., "New parallaxes and a convergence analysis for the TW Hya association," *Astrophysical Journal*, Vol. 833, No. 1, 2016.
18. Johnson, P. V., J. Kim, and M. S. Banks, "Stereoscopic 3D display technique using spatiotemporal interlacing has improved spatial and temporal properties," *Optics Express*, Vol. 23, No. 7, 9252, 2015.
19. Mphepö, W., Y. P. Huang, and H. P. D. Shieh, "Enhancing the brightness of parallax barrier based 3D flat panel mobile displays without compromising power consumption," *Journal of Display Technology*, Vol. 6, No. 2, 60–64, 2009.
20. Kim, S. K., K. H. Yoon, S. K. Yoon, et al., "Parallax barrier engineering for image quality improvement in an autostereoscopic 3D display," *Optics Express*, Vol. 23, No. 10, 13230–44, 2015.
21. Yoon, K. H., H. Ju, H. Kwon, I. Park, et al., "Diffraction effects incorporated design of a parallax barrier for a high-density multi-view autostereoscopic 3D display," *Optics Express*, Vol. 24, No. 4, 4057, 2016.
22. Kim, H., J. Hahn, and H. J. Choi, "Numerical investigation on the viewing angle of a lenticular three-dimensional display with a triplet lens array," *Applied Optics*, Vol. 50, No. 11, 1534–40, 2011.
23. Mumberson, S., "Persistence of vision," *Computer Science & Communications Dictionary*, Vol. 35, No. 1, 44–44, 2004.
24. Fan, H., Y. Zhou, J. Wang, et al., "Full resolution, low crosstalk, and wideviewing angle autostereoscopic display with a hybrid spatial-temporal control using free-form surface backlight unit," *Journal of Display Technology*, Vol. 11, No. 7, 620–624, 2015.
25. Wang, P. C., S. L. Hwang, H. Y. Huang, et al., "System cross-talk and three-dimensional cue issues in autostereoscopic displays," *J. Electron. Imaging*, Vol. 22, No. 1, 013032, 2013.
26. Kooi F. L. and A. Toet, "Visual comfort of binocular and 3D displays," *Displays*, Vol. 25, No. 2–3, 99–108, 2004.
27. Wang, J., H. Liang, H. Fan, et al., "High-quality autostereoscopic display with spatial and sequential hybrid control," *Applied Optics*, Vol. 52, No. 35, 8549–53, 2013.
28. Liang, H., S. An, J. Wang, et al., "Optimizing time-multiplexing auto-stereoscopic displays with a genetic algorithm," *Journal of Display Technology*, Vol. 10, No. 8, 695–699, 2014.
29. Zhou, Y., H. Fan, K. Li, et al., "Simulation and control of display uniformity in a backlight illuminated image array," *Journal of Display Technology*, Vol. 12, No. 7, 355–362, 2016.

30. Li, K., H. Fan, J. Wang, et al., "Visual effect of a linear Fresnel lens illuminated with a directional backlight," *Journal of the Optical Society of America A*, Vol. 33, No. 6, 1155, 2016.
31. Jacobs, D. H., "The stiles-crawford effect and the design of telescopes," *J. Opt. Soc. Amer.*, Vol. 34, No. 11, 694–694, 1944.
32. Moon, P. and D. E. Spencer, "On the stiles-crawford effect," *J. Opt. Soc. Amer.*, Vol. 34, No. 6, 319–329, 1944.
33. Kong, L., G. Jin, and T. Wang, "Analysis of Moiré minimization in autostereoscopic parallax displays," *Opt. Express*, Vol. 21, No. 22, 26068–26079, 2013.
34. Saveljev, V. V., J. Y. Son, B. Javidi, et al., "Moiré minimization condition inthree-dimensional image displays," *J. Disp. Technol.*, Vol. 1, No. 2, 347–353, 2005.
35. Kim, Y., G. Park, J.-H. Jung, et al., "Color moiré pattern simulation and analysis in three-dimensionalintegral imaging for finding the moiré-reduced tilted angle of a lens array," *Appl. Opt.*, Vol. 48, No. 11, 2178–2187, 2009.
36. Zhou, Y., P. Krebs, H. Fan, et al., "Quantitative measurement and control of optical Moiré pattern in an autostereoscopic liquid crystal display system," *Applied Optics*, Vol. 54, No. 6, 1521–7, 2015.
37. Zhou, Y., H. Fan, S. An, et al., "Pseudo-random arranged color filter array for controlling moiré patterns in display," *Optics Express*, Vol. 23, No. 23, 29390, 2015.
38. Laurent, B., B. Ousman, T. Dzudie, et al., "Digital camera images processing of hard-to-cook beans," *Journal of Engineering & Technology Research*, Vol. 2, 177–188, 2010.